Peer reviewed:

Under review

Title:

Travelling wave solutions for the Richards equation incorporating non-equilibrium effects in the capillarity pressure

Author:

C.J. van Duijn[1,2], K. Mitra[3,4], and I.S. Pop[4,5]
1. Eindhoven University of Technology, Department of Mechanical Engineering
2. University of Utrecht, Department of Earth Sciences
3. Eindhoven University of Technology, Department of Mathematics and Computer Science
4. Hasselt University, Faculty of Science
5. University of Bergen, Department of Mathematics

Publication date:

10-2017

Copyright information:

Travelling wave solutions for the Richards equation incorporating non-equilibrium effects in the capillarity pressure

C.J. van Duijn [1,2], K. Mitra*[3,4], and I.S. Pop[4,5]

[1] *Eindhoven University of Technology, Department of Mechanical Engineering*
[2] *University of Utrecht, Department of Earth Sciences*
[3] *Eindhoven University of Technology, Department of Mathematics and Computer Science*
[4] *Hasselt University, Faculty of Science*
[5] *University of Bergen, Department of Mathematics*

Abstract

The Richards equation is a mathematical model for unsaturated flow through porous media. This paper considers an extension of the Richards equation, where non-equilibrium effects like hysteresis and dynamic capillarity are incorporated in the relationship that relates the water pressure and the saturation. The focus is on travelling wave solutions, for which the existence is investigated first for the model including hysteresis and subsequently for the model including dynamic capillarity effects. In particular, such solutions may have non monotonic profiles, which are ruled out when considering standard, equilibrium type models, but have been observed experimentally. The paper ends with numerical experiments confirming the theoretical results.

1 Introduction

Unsaturated flow through porous media is encountered in many applications of societal and engineering relevance. Examples in this sense are the groundwater flows, or the moisture dynamics in building materials. A commonly used mathematical model for such kind of processes is the Richards equation, which is obtained after inserting the Darcy law into the water mass balance equation. The two main unknowns in this equation are the water saturation S (the fraction of the pore space in a representative elementary volume that is occupied by water) and the water pressure p. In standard porous media flow models, these two unknowns are related through the strictly decreasing capillary pressure function $P_c(\cdot)$, namely $p = -P_c(S)$, which is determined experimentally. Different types of functions and parameterizations are discussed e.g. in [31], the common assumption being that the dependence is obtained under special, equilibrium conditions. More precisely, the experiments are carried out either for imbibition or for drainage and not when these processes occur alternatively, and during an entire imbibition or drainage cycle each measurement has been done only after water stops redistributing inside the pores of the elementary volumes. Such models will therefore be called in what follows "equilibrium type models".

In realistic applications, neither of these conditions are met. First, experiments reported e.g. in [15, 29] have revealed the hysteretic nature of the pressure-saturation relationship. More precisely, it was observed that the functions P_c determined during infiltration and drainage

*Corresponding author: email: k.mitra@tue.nl

are different. This motivated an extremely rich literature on mathematical models describing hysteresis. The play-type hysteresis model assumes a switch between imbibition and drainage capillary pressure-saturation curves whenever the saturation changes from increasing in time to decreasing in time or vice-versa. A mathematical formulation of this is given in [3], and the switch happens along vertical scanning curves. This poses nontrivial issues when analysing the resulting models and their numerical discretisations, which can be resolved by approximating the vertical scanning curves by monotone and non-vertical ones. In this sense, commonly used is the Lenhard-Parker model [33], where the scanning curves are rescaled versions of some predefined curves. A simplified version of it is proposed in [10], where the scanning curves are oblique lines. Also extension of play-type hysteresis model incorporating the non-vertical scanning curves has been proposed in [48]. Other hysteresis models build on concepts like percolating/nonpercolating phases [20, 24], or interfacial area based models [30, 35]. An overview of hysteresis models can be found in [51], whereas details on the numerical approximation of hysteresis in porous media models are given in [32]. In the present paper we consider the play-type hysteresis model for the pressure-saturation dependence but it is interesting to note that hysteresis can also be present in the relative permeability curve [34]. However, in the latter case this effect is less important in comparison to the former [15].

Second, when letting the water infiltrate in a homogeneous medium, experiments have revealed profiles that are conflicting with the profiles of the solutions to the equilibrium type models. For example, if the injection rates at the inflow are high enough, the obtained saturation profiles are non-monotone as the values at some locations inside the column are higher than at the inflow boundary (the so-called overshoot phenomenon, see [18]). In particular, the experiments in [7] show that although the saturation at some certain location is decreasing in time, the water pressure is non-monotone and exhibits a peak at moments when the saturation changes rapidly. This pleads for the inclusion of dynamic effects in the pressure-saturation relationship, as suggested in [22].

In mathematical terms, models like those mentioned above are evolution equations of pseudo-parabolic type, or involve differential inclusions. Such models will be called below "non-equilibrium type models". In this paper, we investigate how the solution profiles for unsaturated flow through a long, homogeneous porous column are affected by such non-equilibrium effects. The analysis is based on travelling waves (TW), allowing to reduce the model first to a nonlinear ordinary differential equation, and then to a dynamical system. This provides insight in the structure and behaviour of the solutions, and in particular how the non-equilibrium regime affects the profiles. The present analysis follows the ideas in [47], which studies the existence of TW solutions for reactive flow and transport models in porous media. In [17] TW solutions are analysed for nonlinear models that are similar to the Richards equation, but where higher order effects are included inspired by the ones describing dynamic capillarity. The nonlinear functions taken in [17] are of power-like type, in particular the flux function is convex. The existence of TW solutions is analysed, and in particular it is shown that oscillations behind the infiltration front may occur, depending on the magnitude of the dynamic effect. A similar analysis, but for two-phase flow models implying convex-concave flux functions is carried out in [44, 46, 49]. Also related are the diffusive-dispersive equations appearing as models for the phase transition dynamics, but in which the higher order terms are in terms of the spatial derivatives only [2, 16]. Though having a different motivation, the associated TW equation is similar to the one for the dynamic capillarity models, in particular since both involve a non-convex nonlinearity in the lower order terms. In this context, in [46] it is proved that the saturation profile may have overshoot in form of a plateau separated by two fronts (infiltration-drainage), similar to the ones obtained in [18]. The dependence of the saturation value at such plateaus on the magnitude of the dynamic effect is proved rigorously in [46], and non-standard entropy conditions are defined

for the shock solutions of the limiting hyperbolic case when the capillary effects are neglected. This analysis is extended to the case of degenerate models in [44, 49]. Due to the degeneracy in the model, the saturation remains between the physically relevant values, but the TW solutions may have discontinuous derivatives. The possibility of encountering non-monotonic TW profiles for various extensions of the Richards equation, including dynamic capillarity models, is evidenced numerically in [19, 21]. Finally, we mention [52] for a numerical study of the saturation and capillary pressure profiles for several of the hysteresis concepts discussed above, combined with dynamic capillarity.

The present analysis consists of three parts. First the existence of TW solutions is analysed for the models involving hysteresis. The TW profiles are obtained by regularising the multi-valued function involved in the hysteretic term. In particular, we analyse the orbits associated with the TW solution in the saturation-pressure plane. We prove that in the initial and the final stages these orbits follow scanning curves that become vertical when the regularisation parameter vanishes, and in between they follow the corresponding primary curves (imbibition/drainage).

Next, the case where dynamic effects are present in the pressure-saturation relationship is discussed. The existence of TW solutions is obtained and criteria ensuring their non-monotonicity are provided. These include also situations where full-saturation is achieved.

In the last part we discuss a numerical scheme for approximating the solution of the nonlinear, pseudo-parabolic partial differential equations modelling the processes described above. The scheme is implicit, so at each time step one has to solve a nonlinear problem. In this context we propose an iterative method which is unconditionally convergent. Finally, numerical results validating the theoretical findings are provided. As will be seen below, the numerical solutions to the original model are reproducing nicely analytically predicted structures and properties of the TW solutions.

2 Mathematical formulation

2.1 Basic equations

We consider the unsaturated water flow in a one-dimensional, homogeneous porous medium. Let t and x denote the time and space variable respectively. Assuming that the medium is vertical so that gravity effects are playing a role, a well accepted model for the flow is the Richards equation [31],

$$\phi \frac{\partial S}{\partial t} = \frac{\partial}{\partial x}\left[\kappa \frac{k(S)}{\mu} \cdot \left(\frac{\partial p}{\partial x} - \rho g\right)\right]. \tag{2.1}$$

The unknowns in the model are the water saturation S and the water pressure p. The relative permeability $k(\cdot)$ is a given, positive and increasing function that characterizes the medium and can be determined experimentally. The other quantities are parameters in the model and are assumed positive and known: μ and ρ are the the water viscosity and density, g is the gravitational acceleration, ϕ is the porosity of the medium, and κ its absolute permeability.

The model is completed by an equation describing the relation between p and S. For standard models, this relation is algebraic,

$$-p = P_c(S),$$

where $P_c(\cdot)$ is a decreasing function. Its specific form is determined experimentally. As mentioned, the results available in the literature assume a local equilibrium and disregard the history of the system.

Here we consider the non-equilibrium model proposed in [3], which combines dynamic effects in the p-S relationship with a simple, play-type hysteresis model. For a mathematical justification of the play-type hysteresis model, based on the pore scale analysis, we refer to [43]. Let $p_{imb}(\cdot)$ and $p_{drn}(\cdot)$ be the primary imbibition and drainage capillary pressure curves [29] respectively. In the absence of the dynamic effects one has

$$P_c(S) = \begin{cases} p_{imb}(S) \text{ for } \partial_t S > 0 \text{ (infiltration)}, \\ p_{drn}(S) \text{ for } \partial_t S < 0 \text{ (drainage)}. \end{cases} \tag{2.2}$$

Combining this with the vertical scanning curves the closure relationship can be written in the compact mathematical form

$$-p \in P^+(S) - P^-(S) \cdot \operatorname{sign}\left(\frac{\partial S}{\partial t}\right), \tag{2.3}$$

where $\operatorname{sign}(\cdot)$ is the multi-valued function (the signum graph)

$$\operatorname{sign}(u) = \begin{cases} 1 & \text{for } u > 0 \\ [-1, 1] & \text{for } u = 0 \\ -1 & \text{for } u < 0. \end{cases} \tag{2.4}$$

The functions P^+, P^- are defined as (also see Figure 1 for an example in the dimensionless framework)

$$P^+ = \frac{1}{2}\left(p_{drn} + p_{imb}\right), \qquad \text{and} \qquad P^- = \frac{1}{2}\left(p_{drn} - p_{imb}\right). \tag{2.5}$$

Regarding dynamic effects we refer to [22]. With τ being a damping parameter and $f(\cdot)$ a damping function (both non-negative), the model combining hysteretic and dynamic effects in the pressure-saturation relationship reads

$$-p \in P^+(S) - P^-(S) \cdot \operatorname{sign}\left(\frac{\partial S}{\partial t}\right) - \tau f(S)\frac{\partial S}{\partial t}. \tag{2.6}$$

In [22], a thermodynamic justification of such models has been given. Also, homogenisation techniques are employed in [8] for justifying the dynamic terms. For experimental studies concerning the value of τ and the shape of the function f we refer to [7].

2.2 Scaling and assumptions

In what follows we assume that water infiltrates in a porous column under both capillary and gravity effects. The column is assumed isotropic and homogeneous, implying that ϕ and κ are constants. We also assume that the column is insulated laterally, so the flow will be essentially one-dimensional, in the direction of the gravity. Since we consider here TW solutions, the column is assumed infinite.

With σ being the air-water surface tension coefficient, we consider the reference quantities

$$p^* = \sigma\sqrt{\frac{\phi}{\kappa}}, \qquad L^* = \frac{p^*}{\rho g}, \qquad T^* = \frac{\mu\phi L^*}{\rho g \kappa}, \qquad \tau^* = \frac{\mu L^2 \phi}{\kappa}, \tag{2.7}$$

and apply the rescaling

$$\tilde{x} = \frac{x}{L^*}, \quad \tilde{p} = \frac{p}{p^*}, \quad \tilde{t} = \frac{t}{T^*}, \quad \tilde{\tau} = \frac{\tau}{\tau^*}. \tag{2.8}$$

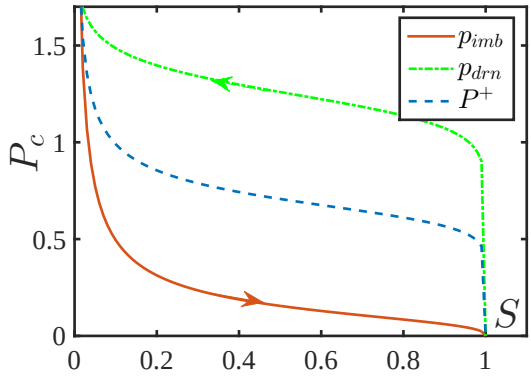

Figure 1: Dimensionless primary imbibition (p_{imb}) and drainage (p_{drn}) capillary pressure curves and their average (P^+) as a function of saturation S. The curves are based on the van Genuchten model [50] and the parameters are taken from experiments [53, p. 91].

Observe that reference value for pressure is inspired by the J-Leverett relationship, $P_c(S) = \sigma\sqrt{\frac{\phi}{k}}J(S)$ where J is decreasing (see, e.g. [45]), and the reference value for the damping parameter τ^* is consistent with [26]. Also, since the analysis below will involve infinite domains, we have first specified a reference pressure and based on it a reference length has been defined. Putting the scaled variables in (2.1) and (2.6) and disregarding the $\tilde{}$ to simplify the notation one obtains the dimensionless system

$$\frac{\partial S}{\partial t} = \frac{\partial}{\partial x}\left[k(S)\left(\frac{\partial p}{\partial x} - 1\right)\right], \tag{2.9}$$

$$-p \in P^+(S) - P^-(S)\cdot \operatorname{sign}\left(\frac{\partial S}{\partial t}\right) - \tau f(S)\frac{\partial S}{\partial t}. \tag{2.10}$$

Next we state the assumptions on the nonlinear functions involved in the model. They reflect the experimental observations. Throughout this paper, the superscript $'$ denotes differentiation with respect to the argument of the function.

(A. 1) $k \in C^1([0,1])$, $k'(S) > 0$ for $0 < S \leq 1$, $k(0) = 0$, $k(1) = 1$ and k is strictly convex.

(A. 2) The damping parameter is positive, $\tau > 0$. The damping function $f \in C([0,1))$ and $f(S) > 0$ for $0 < S < 1$.

(A. 3) The capillary pressure functions p_α, $\alpha \in \{imb, drn\}$ satisfy $p_\alpha : (0,1] \to [0,\infty)$, $p_\alpha \in C^1((0,1])$, $p_\alpha(1) = 0$, $p'_\alpha(S) < 0$ and $p_{imb}(S) < p_{drn}(S)$ for $S \in (0,1)$.

An immediate consequence is that the functions $P^\pm(\cdot)$ defined in (2.5) are in $C^1((0,1])$, satisfying $P^\pm(1) = 0$ and $P^\pm(S) > 0$ for all $S \in (0,1)$. Figure 1 displays an example of primary drainage and imbibition curves and their average P^+.

To analyse the effect of hysteresis, which is modelled by means of a multi-valued function, we consider a regularisation approach. With $\varepsilon > 0$ being a small regularisation parameter, one can approximate the sign function by $H_\varepsilon : \mathbb{R} \to \mathbb{R}$ satisfying the following

(A. 4) For each $\varepsilon > 0$, H_ε is smooth and satisfies

$$H_\varepsilon(-s) = -H_\varepsilon(s) \text{ and } 0 < H'_\varepsilon(s) \leq H'_\varepsilon(0) = \frac{1}{\varepsilon} \text{ for all } s \in \mathbb{R};$$

and

$$\lim_{s\to\pm\infty} H_\varepsilon(s) = \pm 1, \quad \lim_{\varepsilon\to 0} H_\varepsilon(s) = \begin{cases} -1 & \text{if } s < 0 \\ 1 & \text{if } s > 0. \end{cases} \tag{2.11}$$

Further, H_ε depends smoothly and monotonically on ε: if $\varepsilon_1 > \varepsilon_2 > 0$ then $|H_{\varepsilon_1}(s)| < |H_{\varepsilon_2}(s)|$ for all $s \neq 0$.

When sign is replaced by H_ε in (2.10), the regularised model for the pressure-saturation relationship becomes

$$-p = P^+(S) - P^-(S) H_\varepsilon\left(\frac{\partial S}{\partial t}\right) - \tau f(S)\frac{\partial S}{\partial t}. \tag{2.12}$$

Such regularisation has been used in [39, 42] for proving the existence of weak solutions to such models, and for developing appropriate numerical schemes.

One may wonder if the regularisation (2.12) has a physical interpretation. In the play-type limit as $\varepsilon \to 0$, a switch from drainage to imbibition is through a vertical scanning curve. Whereas when considering the regularised model (2.12), scanning curves have a steep but finite slope as observed in experiments [29].

Another motivation for considering regularised models can be found in [51], where the play-type hysteresis is viewed as a 'friction-controlled backslash' process. This means that dissipative forces, which are mostly continuous in porous media, are responsible for it. At the pore scale, hysteresis occurs because of the difference in the advancing and receding contact angles of the wetting phase, which is a continuous phenomenon and hence jump phenomena should not be expected.

Hence ε can be seen as a physical parameter, or at least can be used to fit more realistic P_c-S scanning curves. Having this in mind, in the subsequent discussions we will analyse first the case $\varepsilon > 0$ and then the limiting case of $\varepsilon \to 0$. Before doing so we mention that (2.9), combined with the constitutive relationship (2.10) or its regularised counterpart (2.12), becomes a nonlinear, pseudo-parabolic equation. In general, one cannot expect that solutions exist in a classical sense. We refer to [5, 6, 12, 13, 14, 25, 28, 27, 41, 42, 43] for results concerning the existence and uniqueness of weak solutions for hysteresis models, dynamic capillarity models, or for models including both effects. In particular we refer to [41, 42, 13] where, as suggested in [3, 4], (2.12) is used to express $\partial_t S$ as a function of S and p. We rely on the same idea for the TW analysis below.

2.3 Travelling wave formulation

To simplify the analysis and to understand the profile of the solutions to the regularised mathematical model (2.9), (2.12) we look for TW solutions. We assume that the solutions have profiles that do not change in time, but travel with a velocity c that will be determined later. Specifically, we extend the domain (the porous medium) to the entire real axis $\mathbb{R}$ and assume that the saturation and the pressure depend on the TW variable $\zeta = ct - x$. Note that this choice is the opposite of $x - ct$ which is commonly used in literature. But our choice is convenient for the analysis below. Moreover, for the ease of presentation, we introduce the negative pressure $u = -p$. In groundwater terms u is called suction. In this paper, however, we still refer to u as pressure. Thus we set

$$S(x,t) = S(\zeta) \quad \text{and} \quad u(x,t) = u(\zeta), \qquad \text{with } \zeta = ct - x. \tag{2.13}$$

The wave velocity $c \in \mathbb{R}$ will be determined later. In terms of ζ, equations (2.9) and (2.12) become

$$cS' = (k(S)(-u' + 1))', \tag{2.14}$$

$$u = P^+(S) - P^-(S)H_\varepsilon(cS') - c\tau f(S)S', \tag{2.15}$$

where $-\infty < \zeta < \infty$. Replacing H_ε by sign and "=" by "$\in$" we get the travelling wave system corresponding to (2.9) and (2.10).

We consider the case where the saturation and the pressure admit horizontal asymptotes at $\pm\infty$, i.e.

$$\lim_{\zeta\to-\infty} S(\zeta) = S_B, \quad \lim_{\zeta\to\infty} S(\zeta) = S_T, \tag{2.16}$$

$$\lim_{\zeta\to-\infty} u(\zeta) = u_B, \quad \lim_{\zeta\to\infty} u(\zeta) = u_T. \tag{2.17}$$

for given saturations S_T, S_B satisfying $0 < S_B < S_T \leq 1$ and for given pressures u_B and u_T. We restrict ourselves to the case $S_B < S_T$ for two reasons:

(i) If a travelling wave exists with $c > 0$, then $S_B < S_T$ describes a wetting (infiltration) front moving from top to bottom through the porous column. This is precisely the physical setting that we aim to describe.

(ii) The convexity of k implies that travelling waves can only exist if $S_B < S_T$. This follows directly from the sign of u' in the (S, u) phase plane.

Integrating (2.14) gives

$$cS + A = k(S)(-u' + 1) \text{ in } \mathbb{R}, \tag{2.18}$$

where A is a constant of integration. Using now (2.16) and (2.17) in (2.18) and (2.15) yields

$$\lim_{\zeta\to\pm\infty} S'(\zeta) = \lim_{\zeta\to\pm\infty} u'(\zeta) = 0.$$

Hence (2.15) implies

$$\lim_{\zeta\to-\infty} u(\zeta) = P^+(S_B) \quad \text{and} \quad \lim_{\zeta\to\infty} u(\zeta) = P^+(S_T),$$

which provides a necessary condition for the existence of TW solutions. We have

Proposition 2.1. *A necessary condition for the existence of TW solutions is that the components in the left and right states are compatible, namely* $u_i = P^+(S_i)$ $(i \in \{T, B\})$.

In what follows, this compatibility condition is always assumed.

Applying boundary conditions (2.16) and (2.17) to (2.18) we get

$$c = \frac{k(S_T) - k(S_B)}{S_T - S_B}, \tag{2.19}$$

$$\text{and } u' = \mathcal{G}(S; S_B, S_T), \tag{2.20}$$

where

$$\mathcal{G}(S; S_B, S_T) = 1 - \frac{c(S - S_B) + k(S_B)}{k(S)} = 1 - \frac{c(S - S_T) + k(S_T)}{k(S)}. \tag{2.21}$$

The last equality uses the wave speed expression (2.19).

In this paper we investigate the effect of hysteresis and dynamic capillarity separately. The combined case will be considered in a future study.

From (2.16),(2.17) and Proposition 2.1 it follows that the points $E_i = (S_i, u_i)$ with $u_i = P^+(S_i)$ and $i \in \{T, B\}$ are equilibria for the dynamical system (2.14),(2.15). Much of the TW analysis will be in terms of orbits in the (S, u) plane, connecting E_B and E_T.

Clearly, the corresponding waves are translation invariant (invariant to shift in ζ). To fix the orbit we impose the normalization

$$S(0) = \frac{1}{2}(S_B + S_T) \text{ and } S(\zeta) < \frac{1}{2}(S_B + S_T) \text{ for all } \zeta < 0. \tag{2.22}$$

We will see later that the inequality in (2.22) is needed as S has oscillating behaviour near S_T when E_T becomes a stable spiral sink. From now on, while discussing travelling waves or orbits, we implicitly assume that (2.22) is satisfied.

3 Capillary hysteresis

Dropping the dynamic terms in (2.15) we have

$$u = P^+(S) - P^-(S)H_\varepsilon(cS'). \tag{3.1}$$

For a given regularisation H_ε satisfying (A.4) we introduce

$$\Phi_\varepsilon(r) = \frac{1}{c}H_\varepsilon^{-1}(r) \text{ for } -1 < r < 1. \tag{3.2}$$

Then Φ_ε satisfies

Proposition 3.1. *$\Phi_\varepsilon : (-1, 1) \to \mathbb{R}$ is a smooth, odd and increasing function satisfying $\Phi'_\varepsilon(0) = \frac{\varepsilon}{c}$ for all $\varepsilon > 0$. Also, given two regularisation parameters $\varepsilon_{1,2}$ such that $\varepsilon_2 > \varepsilon_1 > 0$ one has $|\Phi_{\varepsilon_1}(r)| < |\Phi_{\varepsilon_2}(r)|$ for all $r \in (-1, 1)$. Finally, $\lim_{\varepsilon\to 0} \Phi_\varepsilon(r) = 0$ for all $r \in (-1, 1)$.*

The proof is straightforward and is omitted. Figure 2 shows a sketch of Φ_ε for different values of ε.

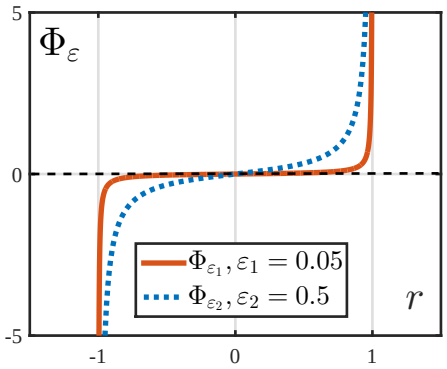

Figure 2: Sketch of Φ_ε. The actual plots are for $\Phi_\varepsilon(r) = \frac{\varepsilon r}{\sqrt{1-r^2}}$ and for the indicated values of ε.

Rewriting (3.1) in terms of Φ_ε we obtain for S and u the dynamical system

$$S' = \Phi_\varepsilon\left(\frac{P^+(S) - u}{P^-(S)}\right), \tag{3.3}$$

$$u' = \mathcal{G}(S; S_B, S_T). \tag{3.4}$$

We consider the cases $S_T = 1$ and $S_T < 1$ separately.

3.1 The case $S_T = 1$

Since $-1 < H_\varepsilon < 1$, equation (3.1) implies for $0 < S < 1$,

$$p_{imb}(S) < u < p_{drn}(S) \tag{3.5}$$

and so

$$-1 < \frac{P^+(S) - u}{P^-(S)} < 1. \tag{3.6}$$

The main result of this section is

Theorem 3.1. *Let $0 < S_B < S_T = 1$ and $E_B = (S_B, P^+(S_B)), E_T = (1, 0)$.*

(a) Let $\varepsilon > 0$ be fixed. The system (3.3)-(3.4) has a unique orbit $(S_\varepsilon, u_\varepsilon)$ connecting the points E_B and E_T. Along the orbit S is increasing and u is decreasing. Consequently, for any $S \in (S_B, 1)$ there exists a unique $\zeta_\varepsilon(S)$ such that $S_\varepsilon(\zeta_\varepsilon(S)) = S$. A similar result holds for $u \in (0, P^+(S_B))$.

(b) The orbits $(S_\varepsilon, u_\varepsilon)$ are well ordered with respect to ε and do not intersect except at the equilibrium points E_B and E_T. Specifically, if $\varepsilon_2 > \varepsilon_1 > 0$ and $S_{\varepsilon_1}(\zeta_1) = S_{\varepsilon_2}(\zeta_2) = S$ for some $S \in (S_B, 1)$ and $\zeta_{1,2} \in \mathbb{R}$, then $u_{\varepsilon_2}(\zeta_1) > u_{\varepsilon_1}(\zeta_2)$.

(c) Let $S \in (S_B, 1]$ be fixed. For arbitrary $\varepsilon > 0$, let $w_\varepsilon(S) := u_\varepsilon(\zeta_\varepsilon(S))$. Then $\lim_{\varepsilon \to 0} w_\varepsilon = p_{imb}(S)$, uniformly on compact subsets of $(S_B, 1]$.

The monotone behaviour of the orbits imply that the TW solutions are monotone in both components. In particular, no overshoot occurs in either pressure or saturation. Moreover the functions $S_\varepsilon : \mathbb{R} \to (S_B, 1)$ and $u_\varepsilon : \mathbb{R} \to (0, P^+(S_B))$ are one to one. This is used in (c) of Theorem 3.1: given $S \in (S_B, 1)$, there exists a unique $\zeta_\varepsilon(S) \in \mathbb{R}$, where $S_\varepsilon(\zeta_\varepsilon(S)) = S$, which defines the corresponding pressure $w_\varepsilon(S) = u_\varepsilon(\zeta_\varepsilon(S))$. The function $w_\varepsilon(S)$, with $S_B < S < 1$ and arbitrary $\varepsilon > 0$, describes the orbits as a function of S. Observe that, the definition of ζ_ε and w_ε makes sense only if S_ε is monotone. If S_ε is not monotone globally, the functions η_ε and w_ε can still be defined but restricted to intervals where the monotonicity of the saturation holds. This generalization will be used to describe the case $S_T < 1$ and for the analysis of dynamic capillarity case.

Differentiation of $w_\varepsilon(S)$ with respect to S gives

$$w'_\varepsilon(S) = \frac{dw_\varepsilon}{dS}(S) = \frac{du_\varepsilon}{d\zeta}(\zeta_\varepsilon)\frac{d\zeta_\varepsilon}{dS_\varepsilon} = \frac{\mathcal{G}(S; S_B, 1)}{\Phi_\varepsilon\left(\dfrac{P^+(S) - w_\varepsilon}{P^-(S)}\right)}. \tag{3.7}$$

To prove Theorem 3.1 we first need some intermediate results. We start with

Proposition 3.2. *The region $H^- = \{(S, u) : S_B < S < 1 \text{ and } p_{imb}(S) < u < P^+(S)\}$ is positive invariant for the dynamical system (3.3)-(3.4).*

Proof. Since $k(\cdot)$ is a convex function it follows that $\mathcal{G}(S; S_B, 1) < 0$ for any $S \in (S_B, 1)$. Also $S'_\varepsilon > 0$ whenever $p_{imb}(S) < u < P^+(S)$. Therefore any orbit $(S_\varepsilon, u_\varepsilon)$ will be monotone in both components as long as it remains in H^-, and the function w_ε introduced above is well defined.

Referring to Figure 3, since $S'_\varepsilon = 0$ and $u'_\varepsilon < 0$ along the graph of P^+, the orbit cannot leave H^- through the upper boundary. The same holds for the vertical boundary $S = S_B$, since along it one has $S'_\varepsilon > 0$. Finally, as the orbit approaches the primary imbibition curve p_{imb} one

has $S'_\varepsilon \to +\infty$ and therefore $\dfrac{dw_\varepsilon}{dS} \to 0$. Since $p'_{imb} < 0$, this implies that the orbit cannot leave H^- through the lower boundary as well. Hence H^- is invariant.

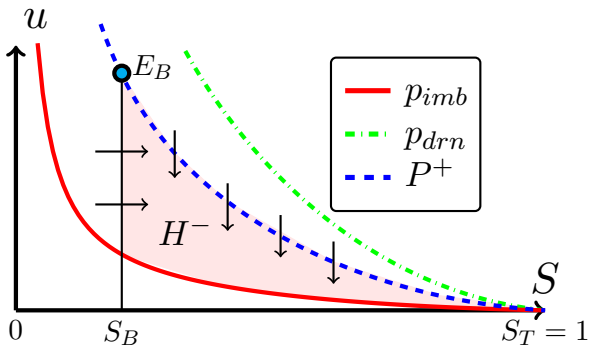

Figure 3: The invariant set H^- in the S-u plane. The arrows indicate direction of orbits with ζ increasing.

□

The next proposition characterises the equilibrium point E_B.

Proposition 3.3. *E_B is a saddle type equilibrium.*

Proof. Linearizing (3.3)-(3.4) around any equilibrium point $E_i = (S_i, P^+(S_i))$ $(i \in \{B, T\})$ yields the characteristic equation

$$\lambda^2 - \Phi'_\varepsilon(0)\frac{P^{+\prime}(S_i)}{P^-(S_i)}\lambda + \Phi'_\varepsilon(0)\frac{(k'(S_i) - c)}{k(S_i)P^-(S_i)} = 0. \tag{3.8}$$

Since k is convex one has $k'(S_B) < c < k'(1)$. Hence at E_B the last term on the left is negative, which proves the result. □

Remark 3.1. Since $\Phi'_\varepsilon(0) = \frac{\varepsilon}{c}$ the positive eigenvalue in 3.8 at E_B, $\lambda = \lambda_{+,B,\varepsilon}$, satisfies

$$\lambda_{+,B,\varepsilon} = \sqrt{{C_1}^2\varepsilon^2 + C_2\varepsilon} - C_1\varepsilon = \mathcal{O}(\sqrt{\varepsilon}), \qquad \text{as } \varepsilon \to 0$$

for appropriately chosen $C_{1,2} > 0$.

We now turn to the proof of Theorem 3.1.

Proof. (a) Consider the situation near the saddle at E_B. A direct calculation shows that the eigenvector corresponding to the unstable eigenvalue $\lambda_{+,B,\varepsilon} > 0$ points into the region H^- for increasing S. Let $(S_\varepsilon, u_\varepsilon)$ be the unique orbit leaving E_B in this direction. By the invariance of H^- and the sign of the right hand sides in (3.3),(3.4), the orbit remains in H^- with increasing S_ε and decreasing u_ε. As $\zeta \to +\infty$ it can only end up in the boundary point $E_T = (1, 0)$.

(b) Letting $S \to S_B$ in (3.7) we obtain

$$w'_\varepsilon(S_B) = \frac{P^{+\prime}(S_B)}{2}\left(1 + \sqrt{1 + \frac{4(c - k'(S_B))P^-(S_B)}{k(S_B)\Phi'_\varepsilon(0)(P^{+\prime}(S_B))^2}}\right). \tag{3.9}$$

Since $\Phi'_\varepsilon(0) = \frac{\varepsilon}{c}$, it follows that $w'_{\varepsilon_1}(S_B) < w'_{\varepsilon_2}(S_B) < 0$ for any $0 < \varepsilon_1 < \varepsilon_2$. Using $w_{\varepsilon_1}(S_B) = w_{\varepsilon_2}(S_B) = P^+(S_B)$ we have $w_{\varepsilon_1}(S) < w_{\varepsilon_2}(S)$ in a right neighbourhood of S_B.

Now suppose there exists $S^* \in (S_B, 1)$ such that $w_{\varepsilon_1}(S^*) < w_{\varepsilon_2}(S^*)$ for $S_B < S < S^*$ and $w_{\varepsilon_2}(S^*) = w_{\varepsilon_1}(S^*)$. Then $w'_{\varepsilon_1}(S^*) \geq w'_{\varepsilon_2}(S^*)$. This contradicts (3.7) at S^*.

(*c*) At this point we know that for all $\varepsilon > 0$,

- $w_\varepsilon(S_B) = P^+(S_B)$, $w_\varepsilon(1) = 0$ and $w_\varepsilon > p_{imb}$ in $(S_B, 1)$.
- For any pair $0 < \varepsilon_1 < \varepsilon_2$, $w_{\varepsilon_1} < w_{\varepsilon_2}$ in $(S_B, 1)$.

As a consequence

$$\lim_{\varepsilon \to 0} w_\varepsilon(S) = \bar{w}(S) \text{ for each } S_B \leq S \leq 1,$$

where $\bar{w} : [S_B, 1] \to [0, P^+(S_B)]$ satisfies $\bar{w}(S_B) = P^+(S_B)$, $\bar{w}(1) = 0$ and $\bar{w}(S) \geq p_{imb}(S)$ for $S_B < S < 1$. Moreover $\bar{w}(S)$ is non-increasing in $[S_B, 1]$, which is inherited from the monotonicity of w_ε in $[S_B, 1]$.

Now suppose there exists $S_0 \in (S_B, 1)$ such that $\bar{w}(S_0) > p_{imb}(S_0)$. Then there exists $\delta > 0$, δ small enough, so that $S_0 - \delta > S_B$ and $w_\varepsilon(S) > w_\varepsilon(S_0) \geq \bar{w}(S_0) > p_{imb}(S_0 - \delta)$ for $S \in (S_0 - \delta, S_0)$. In this situation, all orbits pass through the region (see Figure 4)

$$\mathcal{R} = \{(S, u) : S_0 - \delta/2 < S < S_0 \text{ and } p_{imb}(S_0 - \delta) < u < P^+(S)\}. \tag{3.10}$$

In $\mathcal{R}$ we have

$$\mathcal{G}(S; S_B, S_T) < -C \text{ for some } C > 0, \tag{3.11}$$

and since $\mathcal{R}$ does not touch p_{imb},

$$m = \sup_{(S,u) \in \mathcal{R}} \left(\frac{P^+(S) - u}{P^-(S)} \right), \text{ with } 0 < m < 1.$$

Using this in (3.7) we find, using the monotonicity of Φ_ε

$$-w'_\varepsilon(S) \geq \frac{C}{\Phi_\varepsilon(m)}, \tag{3.12}$$

for all $\varepsilon > 0$ and for $S_0 - \frac{\delta}{2} < S < S_0$. Integration from $S = S_0 - \frac{\delta}{2}$ to $S = S_0$ gives

$$\frac{C\delta}{2\Phi_\varepsilon(m)} \leq w_\varepsilon\left(S_0 - \frac{\delta}{2}\right) - w_\varepsilon(S_0) < P^+(S_B) - P_{imb}(S_0).$$

Letting $\varepsilon \to 0$ we reach a contradiction. Hence $\bar{w}(S) = p_{imb}(S)$ for $S_B < S \leq 1$. By Dini's Theorem the convergence is uniform on any closed interval $[S_B + \mu, 1]$ with $\mu > 0$. □

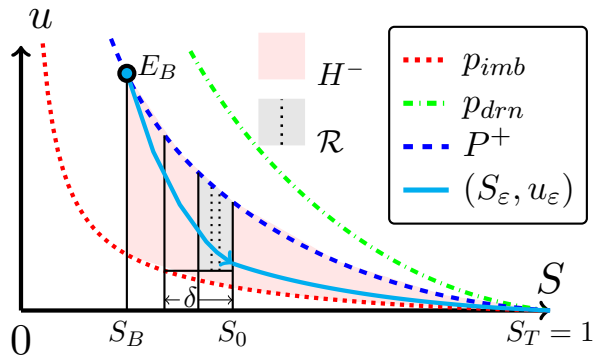

Figure 4: The saturation S_0 and the region $\mathcal{R}$ for $\varepsilon > 0$.

Passing the limit $\varepsilon \to 0$ gives the TW solutions that corresponds to the play-type hysteresis. In terms of saturation $S = S(\zeta)$ it runs from $S = S_B$ as $\zeta \to -\infty$ to $S = S_T = 1$ as $\zeta \to \infty$, while $u = p_{imb}(S)$. We make this precise in the following corollary

Corollary 3.1. *Let $\zeta^*_\varepsilon \in \mathbb{R}$ be such that $u_\varepsilon(\zeta^*_\varepsilon) = p_{imb}(S_B)$ and let $S^*_\varepsilon = S_\varepsilon(\zeta^*_\varepsilon)$. Then*

$$\lim_{\varepsilon \to 0} S^*_\varepsilon = S_B \quad \text{and} \quad \lim_{\varepsilon \to 0} \zeta^*_\varepsilon = -\infty.$$

Before giving the proof we observe that in view of the convergence result in Theorem 3.1 (c), this corollary shows that for $\varepsilon \searrow 0$ the orbits become vertical when approaching E_B.

Proof. Since the orbits $(S_\varepsilon, u_\varepsilon)$ are ordered, S^*_ε decreases with ε. Moreover, by construction $S^*_\varepsilon > S_B$. Hence $\lim_{\varepsilon\to 0} S^*_\varepsilon = S^*$ exists. Assuming $S^* > S_B$ leads to a contradiction as in the proof of Theorem 3.1 (c). Thus $S^* = S_B$.

To prove the second statement we first write equation 3.3 in terms of ζ_ε, ζ_ε being defined in Theorem 3.1 (a):

$$\frac{d\zeta_\varepsilon}{dS}(S) = \frac{1}{\Phi_\varepsilon\left(\dfrac{P^+(S) - w_\varepsilon(S)}{P^-(S)}\right)}. \tag{3.13}$$

As $S^*_\varepsilon = S(\zeta^*_\varepsilon)$ and $S_\varepsilon(0) = (S_B + S_T)/2$, integrating (3.13) and using (3.7) we get

$$-\zeta^*_\varepsilon = \int_{S^*_\varepsilon}^{S_\varepsilon(0)} \frac{dS}{\Phi_\varepsilon\left(\frac{P^+(S)-w_\varepsilon(S)}{P^-(S)}\right)} = \int_{S^*_\varepsilon}^{S_\varepsilon(0)} \frac{w'_\varepsilon(S)}{\mathcal{G}(S; S_B, 1)} dS.$$

Since $S^*_\varepsilon \to S_B$, for any $\delta > 0$ there exists a $\bar\mu = \bar\mu(\delta)$ such that $S_B < S^*_\varepsilon < S_B + \delta$ for all $0 < \varepsilon < \bar\mu(\delta)$. Using $\mathcal{G} \in C^1([S_B, 1])$ and $M_{\mathcal{G}} = \max\{|\mathcal{G}'(S)| : S \in [S_B, \frac{1}{2}(S_T + S_B)]\}$ we estimate

$$-\zeta^*_\varepsilon \geq \frac{1}{M_{\mathcal{G}}} \int_{S^*_\varepsilon}^{S_\varepsilon(0)} \frac{-w'_\varepsilon(S)}{S - S_B} dS \geq \frac{1}{M_{\mathcal{G}}} \int_{S_B+\delta}^{\frac{1}{2}(S_T+S_B)} \frac{-w'_\varepsilon(S)}{S - S_B} dS =: \frac{1}{M_{\mathcal{G}}} h_\varepsilon. \tag{3.14}$$

Evaluating h_ε gives

$$h_\varepsilon = \frac{w_\varepsilon(S_B + \delta)}{\delta} - \frac{2w_\varepsilon(\frac{1}{2}(S_T + S_B))}{(S_T - S_B)} - \int_{S_B+\delta}^{\frac{1}{2}(S_T+S_B)} \frac{w_\varepsilon(S)}{(S - S_B)^2} dS.$$

Since w_ε converges uniformly in $[S_B + \delta, \frac{1}{2}(S_B + S_T)]$ and since $p_{imb} \in C^1$ we have

$$\begin{aligned}\lim_{\varepsilon\to 0} h_\varepsilon &= \frac{p_{imb}(S_B + \delta)}{\delta} - \frac{2p_{imb}(\frac{1}{2}(S_T + S_B))}{S_T - S_B} - \int_{S_B+\delta}^{\frac{1}{2}(S_T+S_B)} \frac{p_{imb}(S)}{(S - S_B)^2} dS \\ &= \int_{S_B+\delta}^{\frac{1}{2}(S_T+S_B)} \frac{-p'_{imb}}{(S - S_B)} dS =: h_0.\end{aligned}$$

Therefore for any $\nu > 0$, there exists a $\mu^*(\nu) > 0$ such that $h_\varepsilon > h_0 - \nu$ for all $\varepsilon \in (0, \mu^*(\nu))$. Thus for $0 < \varepsilon < \min\{\bar\mu(\delta), \mu^*(\nu)\}$

$$-\zeta^*_\varepsilon \geq \frac{1}{M_{\mathcal{G}}}(h_0 - \nu) \geq \frac{M_p}{M_{\mathcal{G}}} \ln\left(\frac{S_T - S_B}{2\delta}\right) - \frac{\nu}{M_{\mathcal{G}}}, \tag{3.15}$$

where $M_p = \min\{-p'_{imb}(S) : S_B < S < \frac{1}{2}(S_B + S_T)\}$. Since δ can be chosen arbitrarily small, this concludes the proof. □

3.2 The case $S_T < 1$

We consider now the case when the top and bottom saturations satisfy $0 < S_B < S_T < 1$. In the analysis we use the region

$$H = \{(S, u) : S_B \leq S \leq 1, p_{imb}(S) \leq u \leq p_{drn}(S)\},$$

and its subregions (see Figure 5)

$$\begin{aligned}H_1 &= \{(S, u) : S_B \leq S \leq S_T, p_{imb}(S) \leq u \leq P^+(S)\}, \\ H_2 &= \{(S, u) : S_T \leq S \leq 1, p_{imb}(S) \leq u \leq P^+(S)\}, \\ H_3 &= \{(S, u) : S_T \leq S \leq 1, P^+(S) \leq u \leq p_{drn}(S)\}, \\ H_4 &= \{(S, u) : S_B \leq S \leq S_T, P^+(S) \leq u \leq p_{drn}(S)\}.\end{aligned}$$

We first analyse the case when $\varepsilon > 0$.

3.2.1 Properties for fixed $\varepsilon > 0$

The key properties of the orbits are stated in

Theorem 3.2. *Let $0 < S_B < S_T < 1$ and $\varepsilon > 0$. Then the following holds*

(a) There exists a unique orbit $(S_\varepsilon, u_\varepsilon)$ satisfying (3.3),(3.4),(2.22) and connecting E_B and E_T.

(b) There exists a $\varepsilon_m > 0$ such that E_T is a stable spiral sink whenever $0 < \varepsilon < \varepsilon_m$.

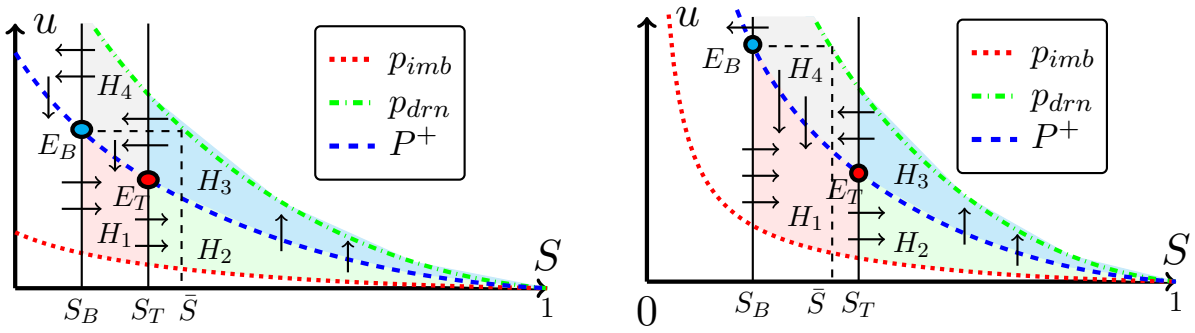

Figure 5: The regions H_1, H_2, H_3 and H_4 for the cases $S_T < \bar{S}$ (left) and $S_T > \bar{S}$ (right) where $\bar{S}$ is defined as $p_{drn}(\bar{S}) = P^+(S_B)$. The arrows indicate direction of orbits with ζ increasing.

Proof. (a) Repeating the proof for the $S_T = 1$ case, we observe that the equilibrium E_B is a saddle and all orbits leaving E_B along the unstable direction and for increasing S_ε enter the region H^- introduced in Proposition 3.2. Also, no orbit can leave the region H defined above through the primary curves $p_{imb}(S)$ and $p_{drn}(S)$. Now we let $\bar{S}$ be such that $p_{drn}(\bar{S}) = P^+(S_B)$. Then two cases can be identified, $S_T < \bar{S}$ and $S_T \geq \bar{S}$.

The case $S_T < \bar{S}$: With respect to Figure 5, the orbit leaving E_B for increasing S_ε enters first the region H_1. Then there are four possibilities (see Figure 5)

1. The orbit goes through H_2, H_3, H_4 and returns to E_B.
2. The orbit goes through H_2, H_3, H_4 and leaves H_4 through the segment (S_B, u_B), $(S_B, p_{drn}(S_B))$.
3. The orbit goes through H_2, H_3, H_4 and then leaves H_4 through the arc $(S, P^+(S))$ between E_B and E_T. This in turn gives rise to two possibilities:

   A. The orbit moves around E_T but does not approach it.
   B. The orbit ends up in E_T.

The case $S_T \geq \bar{S}$: In this case, if the orbit enters from H_3 to H_4 at some $\zeta = \zeta_{3\text{-}4}$, $u_\varepsilon(\zeta_{3\text{-}4}) < p_{drn}(S_T) < p_{drn}(\bar{S}) = u_B$. But in H_4, u_ε is decreasing, hence $u_\varepsilon < u_B$ for all arguments $\zeta > \zeta_{3\text{-}4}$, which rules out the first two possibilities (possibility 1 and 2) above.

To show that actually 3.B is the only possibility in both cases, we follow an argument from [17], based on Divergence Theorem. We define the vector-valued function

$$\mathbf{F} : H \to \mathbb{R}^2, \quad \mathbf{F}(S, u) = (\Phi_\varepsilon(S, u), \mathcal{G}(S)), \tag{3.16}$$

and denote its components by $\mathbf{F}_S$ and $\mathbf{F}_u$ respectively. A direct calculation gives

$$\nabla \cdot \mathbf{F} = \frac{\Phi'_\varepsilon}{(P^-)^2} \cdot (P^{+'} P^- - P^+ P^{-'} + u P^{-'}),$$

where the arguments S and u are disregarded. Hence, for $(S,u) \in H$ one has

$$\nabla \cdot \mathbf{F}(S,u) < \begin{cases} \dfrac{\Phi_\varepsilon'}{(P^-)^2} \cdot (P^{+'}P^- - P^+P^{-'} + P^{-'}p_{imb}) \text{ if } P^{-'}(S) < 0 \\ \dfrac{\Phi_\varepsilon'}{(P^-)^2} \cdot (P^{+'}P^- - P^+P^{-'} + P^{-'}p_{drn}) \text{ if } P^{-'}(S) > 0 \end{cases}$$

The last factor in the first inequality gives

$$\begin{aligned} &\frac{1}{4}(p_{drn}+p_{imb})'(p_{drn}-p_{imb}) - \frac{1}{4}(p_{drn}+p_{imb})(p_{drn}-p_{imb})' + \frac{p_{imb}}{2}(p_{drn}-p_{imb})' \\ &= \frac{1}{4}(2p_{drn}p_{imb}' - 2p_{imb}p_{imb}') = \frac{1}{2}(p_{drn}-p_{imb})p_{imb}' < 0 \end{aligned}$$

Similarly, in the second inequality one gets $\frac{1}{2}(p_{drn}-p_{imb})p_{drn}' < 0$. Thus we have shown that

$$\nabla \cdot \mathbf{F}(S,u) < 0 \quad \text{for all } (S,u) \in H. \tag{3.17}$$

We can now investigate the possibilities mentioned above. To rule out the first two possibilities

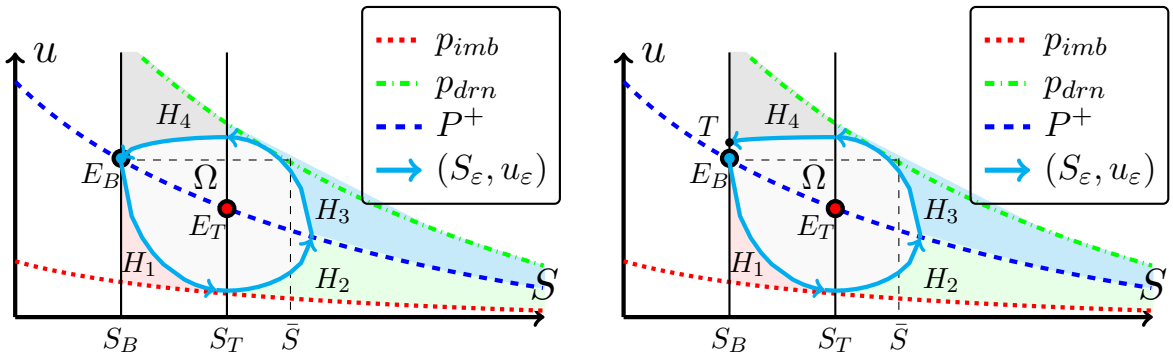

Figure 6: Possibility 1 (left) : orbit returning to E_B after going through regions H_1, H_2, H_3 and H_4. Possibility 2 (right) : orbit exiting region H_4 through the segment (S_B, u_B), $(S_B, p_{drn}(S_B))$.

in the case $S_T < \bar{S}$ we define the domain Ω bounded by the closed orbit, or by the orbit and the segment (S_B, u_B), $(S_B, p_{drn}(S_B))$ (see Figure 6). Let the orbit intersect the segment (S_B, u_B), $(S_B, p_{drn}(S_B))$ at the point T. So for possibility 1, T is simply E_T. By (3.17) one has

$$0 > \int_\Omega \nabla \cdot \mathbf{F} = \int_{E_B}^{T} \mathbf{F} \cdot \hat{n} + \int_{T}^{E_B} \mathbf{F} \cdot \hat{n} = 0 - \int_{T}^{E_B} \mathbf{F}_S,$$

with the last integral on the right appearing only in the second possibility listed above. Since $\mathbf{F}_S \leq 0$ in the region $H \backslash H^-$, this gives a contradiction.

Finally, to eliminate 3.A we observe that by the Poincaré-Bendixson Theorem, if the orbit does not end up in E_T then it must approach a limit cycle around E_T. However, one can use again the argument above, to show that limit cycles do not exist. So, the only possible behaviour of the orbits is as stated in possibility 3.B. This is displayed in the left plot of Figure 7. Also this orbit is unique if condition (2.22) is taken into account as this clearly fixes $\zeta = 0$.

(b) Having proved the existence of an orbit connecting E_B and E_T, showing that the orbit forms a stable spiral around E_T for small enough ε is a matter of calculation. Using the properties of Φ_ε, P^+ and the convexity of k in (3.8) it is easy to show that for small values of ε, the eigenvalues corresponding to equilibrium point E_T will be complex with negative real part. This completes the proof. □

The left plot in Figure 7 shows the phase portrait in the S-u plane. In the right plot one has orbit component S as function of $-\zeta$, in the case when E_T is a stable spiral. Note the usage of $-\zeta = x - ct$ instead of ζ, which is because in the original problem (with x and t as independent variables) the left state ($x = -\infty$) corresponds to S_T and right state ($x = \infty$) corresponds to S_B. This convention is used when comparing with numerical solutions to (2.9)-(2.12).

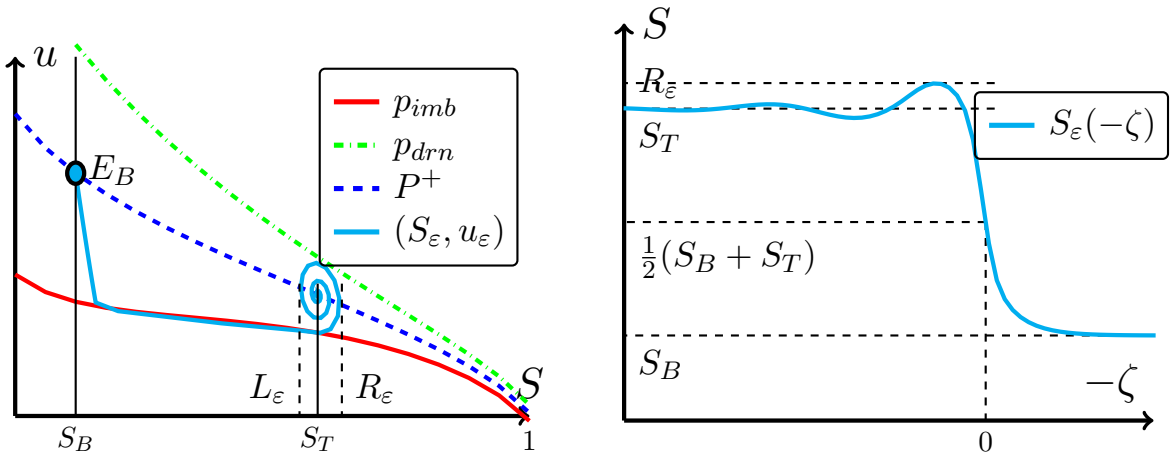

Figure 7: (left) Orbit connecting the saddle point to the spiral sink E_T, and (right) the profile of S as a function of $-\zeta = x - ct$. The results shown, are for $\varepsilon < \varepsilon_m$.

3.2.2 Properties for the limit case $\varepsilon \to 0$

Knowing now the structure of the orbits for fixed $\varepsilon > 0$, we study their behaviour as $\varepsilon \to 0$. In certain aspects, the results obtained for $S_T = 1$ and for $S_T < 1$ are quite similar. The major difference is in the fact that the orbits are not monotone anymore. Consequently, the function w_ε introduced Theorem 3.1 can only be defined as long as S_ε remains monotone. Clearly, when starting from E_B the monotonicity is lost for the first argument ζ where $S_\varepsilon(\zeta) = S_T$. We define ζ_ε^T as

$$\zeta_\varepsilon^T = \min\{\zeta \in \mathbb{R} : S_\varepsilon(\zeta) = S_T\}. \tag{3.18}$$

From now on we refer to the function w_ε as the one obtained for $\zeta \in (-\infty, \zeta_\varepsilon^T]$. With this, one has

Proposition 3.4. *(a) As long as $S \le S_T$ the orbits $(S_\varepsilon, u_\varepsilon)$ are well ordered with respect to $\varepsilon > 0$, and do not intersect.*

(b) For any $S \in (S_B, S_T]$, $w_\varepsilon(S) \to p_{imb}(S)$ as $\varepsilon \to 0$, uniformly on compact subsets of $(S_B, S_T]$.

The proof is the same as for Theorem 3.1 and is therefore omitted here.

For the case $S_T = 1$, Corollary 3.1 is stating the limit behaviour of the orbits when $\varepsilon \searrow 0$. The nature of the equilibrium E_B remains unchanged when $S_T < 1$. Therefore similar results hold as before: if $\zeta_\varepsilon^* \in \mathbb{R}$ is such that $u_\varepsilon(\zeta_\varepsilon^*) = p_{imb}(S_B)$, for $S_\varepsilon^* = S_\varepsilon(\zeta_\varepsilon^*)$ one has

$$\lim_{\varepsilon \to 0} S_\varepsilon^* = S_B \quad \text{and} \quad \lim_{\varepsilon \to 0} \zeta_\varepsilon^* = -\infty,$$

and the corresponding orbits become vertical when approaching E_B.

The situation changes for E_T since the orbits $(S_\varepsilon, u_\varepsilon)$ form stable spirals for small ε. To understand this behaviour we let $\bar{\zeta}_\varepsilon = \min\{\zeta \in \mathbb{R} : S_\varepsilon(\zeta) = S_T\}$ and define (see Figure 7 (left))

$$R_\varepsilon = \sup\{S_\varepsilon(\zeta) : u_\varepsilon(\zeta) = P^+(S_\varepsilon(\zeta))\} \text{ and } L_\varepsilon = \inf\{S_\varepsilon(\zeta) : u_\varepsilon(\zeta) = P^+(S_\varepsilon(\zeta)), \zeta > \bar{\zeta}_\varepsilon\}.$$

The following statement is proved

Proposition 3.5. *For $\bar{\zeta}_\varepsilon$, L_ε and R_ε introduced above, one has*

$$\lim_{\varepsilon\to 0} \bar{\zeta}_\varepsilon = \infty, \quad \lim_{\varepsilon\to 0} L_\varepsilon = S_T \quad \text{and} \quad \lim_{\varepsilon\to 0} R_\varepsilon = S_T.$$

Proof. The proof for $\bar{\zeta}_\varepsilon$ is almost identical to the proof of Corollary 3.1. For the remaining part we only consider R_ε, the proof for L_ε being similar.

Clearly, $R_\varepsilon \geq S_T$. Assuming that a $\delta > 0$ and a sequence $\varepsilon_k \to 0$ exist such that $R_{\varepsilon_k} > S_T + \delta$ for all $k \in \mathbb{N}$. Let

$$\mathcal{R} = \left\{(S, u) : S_T + \frac{\delta}{2} < S < S_T + \delta \text{ and } p_{imb}(S_T) \leq u \leq P^+(S)\right\}.$$

Clearly, all orbits pass through $\mathcal{R}$. Letting

$$M = \sup_{(S,u)\in\mathcal{R}} \left(\frac{P^+(S) - u}{P^-(S)}\right)$$

one has $0 \leq M < 1$ and $0 \leq \Phi_\varepsilon\left(\frac{P^+(S)-u}{P^-(S)}\right) < \Phi_\varepsilon(M)$ for all $(S, u) \in \mathcal{R}$. From (3.7) and recalling that k is convex, for any $S \in \left(S_T + \frac{\delta}{2}, S_T + \delta\right)$ one has

$$w'_{\varepsilon_k}(S) > \frac{\mathcal{G}(S; S_B, S_T)}{\Phi_{\varepsilon_k}(M)} > \frac{(k(S) - k(S_T)) - c(S - S_T)}{k(S_T + \delta) \cdot \Phi_{\varepsilon_k}(M)}.$$

Integrating the above over $\left(S_T + \frac{\delta}{2}, S_T + \delta\right)$ and using the properties of k, a constant $C_0 > 0$ depending on δ but not on ε exists such that

$$w_{\varepsilon_k}(S_T + \delta) - w_{\varepsilon_k}\left(S_T + \frac{\delta}{2}\right) > \frac{C_0}{\Phi_{\varepsilon_k}(M)}.$$

In the above, the difference on the left is bounded by $P^+(S_T) - p_{imb}(S_T + \delta)$. However, by Proposition 3.1, the ratio on the right goes to ∞ when $\varepsilon \to 0$, which gives a contradiction. This implies that $R_\varepsilon \to S_T$ for $\varepsilon \searrow 0$. □

Summarising we have for the behaviour of $S_\varepsilon(\zeta)$ as $\varepsilon \to 0$

Proposition 3.6. *The limit solution $(S(\zeta), p_{imb}(S(\zeta)))$ solves the following boundary value problem*

$$cS' = [k(S)((p_{imb}(S))' + 1)], \quad S(-\infty) = S_B, \quad S(\infty) = S_T.$$

Proof. From (3.13) we get that

$$\zeta_\varepsilon(S) = -\int_{\frac{1}{2}(S_B+S_T)}^{S} \frac{w'_\varepsilon(S)}{\mathcal{G}(S)} dS. \tag{3.19}$$

Following the exact steps produced in Corollary 3.1, i.e. integrating by parts (3.19) and then using $\lim_{\varepsilon\to 0} w_\varepsilon(S) = p_{imb}(S)$, one obtains that the limit

$$\zeta_0(S) = \lim_{\varepsilon\to 0} \zeta_\varepsilon(S),$$

exists. Moreover $\zeta_0(S)$ depends continuously and strictly monotonically on S for all $S \in (S_B, S_T)$ and $\zeta_0(S_B) = -\infty$, $\zeta_0(S_T) = \infty$, the last one following from Proposition 3.5. This means for any $\zeta \in \mathbb{R}$ one can find a $S = \zeta_0^{-1}(\zeta)$. This makes the solution $S(\zeta)$ well defined. Differentiating the limit version of (3.19) with respect to S and inverting we get

$$\frac{dS}{d\zeta}(\zeta) = -\frac{\mathcal{G}(S(\zeta))}{p'_{imb}(S(\zeta))}. \tag{3.20}$$

Rearranging terms completes the proof. □

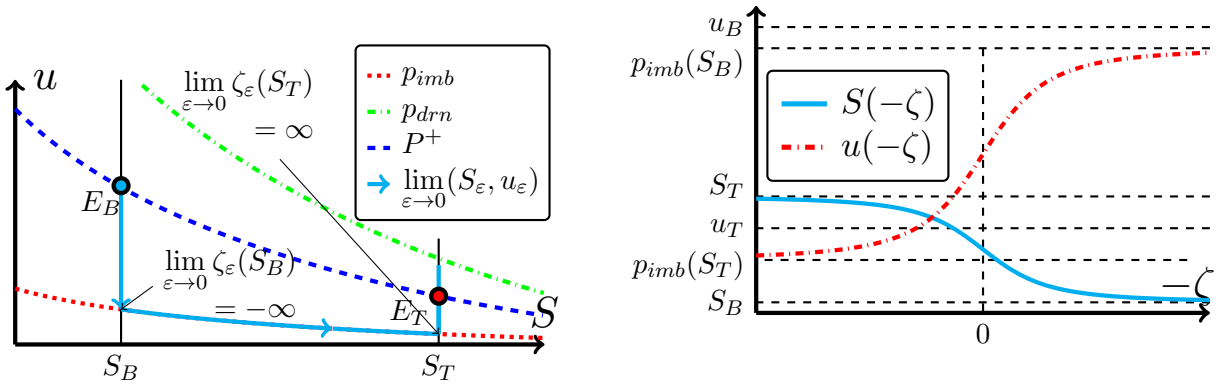

Figure 8: Orbit for limiting case $\varepsilon \to 0$ in S-u plane (left); and saturation and pressure profiles for the limiting orbit as a function of $-\zeta = x - ct$ (right).

Remark 3.2. Propositions 3.4, 3.5 and 3.6 characterise the behaviour of the orbits in the limiting case $\varepsilon \to 0$. These orbits are approaching vertical segments at $S = S_B$ and $S = S_T$, and in between the primary imbibition curve (see Figure 8). Possible oscillations can appear around E_T when $S_T < 1$. As $\varepsilon \to 0$, these oscillations are damped in the S component, but we are unable to show a similar behaviour for the pressure. Computational results shown in Figures 19 and 20 indicate that pressure oscillations do not decay as ε decreases. However, these oscillations cannot be observed in reality for $\varepsilon \to 0$ as they are pushed towards infinity. Proceeding as in Corollary 3.1, one can show that $\zeta_\varepsilon^* \to -\infty$ as $\varepsilon \to 0$ and a similar result holds for the other side, determined by S_T. In other words, the oscillations move to infinity and at any finite point the limiting waves are monotone in both saturation and pressure and they lie on the primary imbibition curve.

4 Dynamic capillarity

Now we discuss the case without hysteresis, but include dynamic effects in the P_c-S relationship. More precisely, we assume that the primary curves in (2.5) are the same, $p_{imb} = p_{drn}$, giving $P^-(S) = 0$ and $P^+(S) = p_{imb}(S)$ for all S. For the ease of presentation, as many results in this case are similar to the ones for the hysteresis model, we still use the notations $P^\pm$.

At the same time we now take $\tau > 0$ and thus (2.10) and (2.12) become $u = P^+(S) - \tau f(S)\partial_t S$. With the TW velocity c given in (2.19), the dynamical system (2.14)-(2.15) associated to the TW solutions become,

$$S' = \frac{P^+(S) - u}{c\tau f(S)}, \tag{4.1}$$

$$u' = \mathcal{G}(S; S_B, S_T). \tag{4.2}$$

As before, we seek orbits that connect the equilibria $E_B = (S_B, P^+(S_B))$ and $E_T = (S_T, P^+(S_T))$, where $0 < S_B < S_T \leq 1$. To fix the orbits we normalize the orbits by assuming that $S(0) = (S_B + S_T)/2$. We remark that this section borrows ideas and extends results from [17, 44, 46, 49].

Before investigating the existence of the TW solutions to the system (4.1)-(4.2) we observe that in certain cases the analysis can be reduced to the simpler case $f \equiv 1$. To see this we introduce the transformed variable

$$Y = Y(S) = \int_0^S f(\varrho) d\varrho. \tag{4.3}$$

Following from Assumption (A.2), this transformation has a unique inverse which we write as $S = S(Y)$. Also, $Y(1) < \infty$ if and only if $f \in L^1(0,1)$. In terms of (Y, u), the system (4.1)-(4.2) becomes

$$Y' = \frac{\tilde{P}^+(Y) - u}{c\tau}, \tag{4.4}$$

$$u' = \tilde{\mathcal{G}}(Y; Y_B, Y_T), \tag{4.5}$$

with $Y_i = \int_0^{S_\ell} f(\varrho) d\varrho$ for $i \in \{B, T\}$ and the functions $\tilde{P}^+, \tilde{\mathcal{G}}$ defined as

$$\tilde{P}^+(Y) = P^+(S(Y)) \text{ and } \tilde{\mathcal{G}}(Y; Y_B, Y_T) = \mathcal{G}(S(Y); S_B, S_T). \tag{4.6}$$

Observe that the system (4.4)-(4.5) is qualitatively similar to (4.1)-(4.2) for the constant damping function, $f \equiv 1$. The difference is in a reinterpretation of the nonlinearities P^+ and $\mathcal{G}$. In view of this we start analysing the existence of TW solutions and their properties by replacing (4.1) with the simpler equation

$$S' = \frac{P^+(S) - u}{c\tau}. \tag{4.7}$$

The more general case when $f \in L^1(0,1)$ is discussed briefly at the end of Subsection 4.1. Moreover, the analysis also extends to cases when $f \notin L^1(0,1)$. As will be seen in Subsection 4.2, the case $f \notin L^1$ gives a natural framework in which the saturation remains within the physically relevant range, $S \in [0,1]$.

4.1 General behaviour of the orbits

As for the hysteresis case, in this part we analyse the existence of orbits of the system (4.7), (4.2) connecting the equilibrium points E_B and E_T. Clearly, these orbits will depend on τ, motivating the notation (S_τ, u_τ). Below we use the regions

$$H_1 = \{(S,u) : S_B \leq S \leq S_T, u \leq P^+(S)\}, \qquad H_2 = \{(S,u) : S_T \leq S \leq 1, u \leq P^+(S)\},$$
$$H_3 = \{(S,u) : S_T \leq S \leq 1, P^+(S) \leq u\}, \qquad H_4 = \{(S,u) : S_B \leq S \leq S_T, P^+(S) \leq u\}.$$

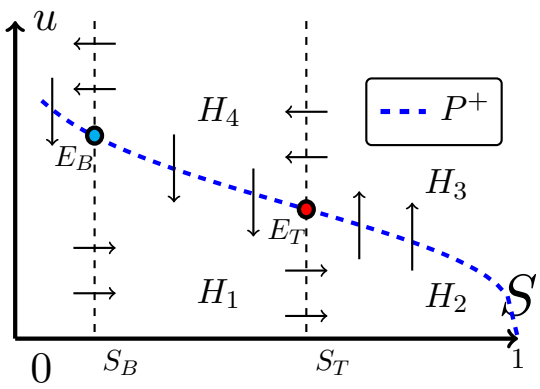

Figure 9: The directions followed by the orbits in the S-u plane for dynamic capillary case.

Figure 9 shows the directions followed by the orbits of the system (4.7), (4.2). Note that if an orbit goes through H_1, there it is monotone in both components, namely $u'_\tau < 0$ and $S'_\tau > 0$. Hence an orbit can only exit H_1 through the line $S = S_T$.

A straightforward calculation shows that the eigenvalues for the linearization of (4.7), (4.2) around $E_i = (S_i, P^+(S_i))$ $(i \in \{B, T\})$ are

$$\lambda_\tau^\pm = \frac{(P^+)'(S_i)}{2c\tau}\left(1 \pm \sqrt{1 - \frac{4c\tau(k'(S_i) - c)}{k(S_i)(P^{+\prime}(S_i))^2}}\right). \tag{4.8}$$

Since k is convex, one has $k'(S_T) > c > k'(S_B)$, which shows that E_B is a saddle point. Further, the unstable orbit leaving E_B to the right enters the region H_1. To understand its behaviour as $\zeta \to \infty$ we begin with

Proposition 4.1. *Given $\tau > 0$, the orbit (S_τ, u_τ) leaving E_B into H_1 either approaches E_T from H_1 as $\zeta \to \infty$, or leaves H_1 through the vertical line $S = S_T$.*

Proof. In view of the monotonicity inside H_1, if (S_τ, u_τ) does not leave H_1 through its right boundary it will approach an equilibrium contained in H_1 and at the right of E_B. Since k is a convex function, the only such point is E_T. □

As for the hysteresis model, all orbits (S_τ, u_τ) are monotone between (S_B, S_T). So, similar to Theorem 3.1, with the stated normalization $S_\tau(0) = (S_B + S_T)/2$, it is possible to define the functions $\zeta_\tau, w_\tau : (S_B, S_T) \to \mathbb{R}$ for the dynamic capillarity model as well. More precisely, for any $S \in (S_B, S_T)$, a unique $\zeta_\tau(S)$ exists such that $S_\tau(\zeta_\tau(S)) = S$ and $S_\tau(\zeta) < S$ for all $\zeta < \zeta_\tau(S)$. With this, $w_\tau(S) = u_\tau(\zeta_\tau(S))$. Also one can extend w_τ to the closed interval $[S_B, S_T]$.

We emphasize on the fact that the functions are defined as long as S_τ remains increasing. In particular, this holds until the orbit leaves $H_1 \cup H_2$. Similar to (3.7), w_τ satisfies the equation

$$w'_\tau(S) = \frac{\tau c \mathcal{G}(S; S_B, S_T)}{P^+(S) - w_\tau}. \tag{4.9}$$

The propositions below explain how the orbits (S_τ, u_τ) depend on τ, before they leave H_1.

Proposition 4.2. *For the family of functions w_τ introduced above one has*

(a) $w_\tau \to P^+$ uniformly in $[S_B, S_T]$ as $\tau \to 0$.

(b) For any $S \in (S_B, S_T]$, $w_\tau(S) \to -\infty$ as $\tau \to \infty$.

Proof. We define the family of functions $v_\tau : [S_B, S_T] \to [0, \infty)$, $v_\tau(S) = P^+(S) - w_\tau(S)$. Note that since $(S_\tau, u_\tau) \in H_1$, v_τ is always positive. By (4.9) we get

$$\frac{1}{2}(v^2)'(S) = vv'(S) = -c\tau\mathcal{G}(S; S_B, S_T) + vP^{+\prime} \le -c\tau\mathcal{G}(S; S_B, S_T). \tag{4.10}$$

Integration from $S = S_B$ to an arbitrary $S \in (S_B, S_T)$ gives

$$v^2(S) \le -2c\tau \int_{S_B}^{S} \mathcal{G}(\varrho; S_B, S_T)d\varrho \le -2c\tau \int_{S_B}^{S_T} \mathcal{G}(\varrho; S_B, S_T)d\varrho = 2\tau\bar{K},$$

with $\bar{K} = -c\int_{S_B}^{S_T} \mathcal{G}(\varrho)d\varrho \geq 0$. This implies

$$0 \leq P^+(S) - w_\tau(S) \leq \sqrt{2\tau\bar{K}}. \tag{4.11}$$

Observing that $\bar{K}$ does not depend on S, the conclusion follows immediately.

For the second part, assume there exists $L > 0$ and $S^* \in (S_B, S_T]$ such that $w_{\tau_k}(S^*) > P^+(S^*) - L$ for a sequence $\{\tau_k\}_{k\in\mathbb{N}}$ going to infinity. Since w_{τ_k} is strictly decreasing in $[S_B, S_T]$ we have $P^+(S) - w_{\tau_k}(S) < P^+(S) - P^+(S^*) + L$ if $S_B < S < S^*$. Since $\mathcal{G}(S; S_B, S_T) < 0$ in H_1 integration of (4.9) gives

$$\begin{aligned} w_{\tau_k}(S^*) &= w_{\tau_k}(S_B) + c\tau_k \int_{S_B}^{S^*} \frac{\mathcal{G}(\varrho)}{P^+(\varrho) - w_{\tau_k}(\varrho)} d\varrho \\ &< P^+(S_B) + c\tau_k \int_{S_B}^{S^*} \frac{\mathcal{G}(\varrho; S_B, S_T)}{P^+(\varrho) - P^+(S^*) + L} d\varrho = P^+(S_B) - c\tau_k K_s, \end{aligned} \tag{4.12}$$

with $K_s = \int_{S_B}^{S^*} \frac{\mathcal{G}(\varrho;S_B,S_T)}{P^+(\varrho)-P^+(S^*)+L} d\varrho$. Clearly, $K_s > 0$. Since $\lim_{k\to\infty} \tau_k = \infty$, this contradicts the assumed boundedness of w_{τ_k} and the proposition is proved. □

The orbits depend continuously and monotonically on τ, as follows from

Proposition 4.3. *For all $S \in [S_B, S_T]$, $w_\tau(S)$ is continuously decreasing with respect to τ.*

Proof. The proof for the monotonicity follows the arguments in the proof of Theorem 3.1 (b) and is omitted.

For the continuity we take $S \in (S_B, S_T]$ and $0 < \tau_1 < \tau_2$, and use again the functions $v_\imath = P^+ - w_{\tau_\imath}$, $\imath \in \{1, 2\}$. From (4.10) and using the monotonicity of w_τ with respect to τ one obtains

$$\frac{1}{2}(v_2^2 - v_1^2)'(S) = -c(\tau_2 - \tau_1)\mathcal{G}(S; S_B, S_T) + (v_2 - v_1)P^{+\prime}(S) < -c(\tau_2 - \tau_1)\mathcal{G}(S; S_B, S_T).$$

With $\bar{K}$ defined above, integration gives

$$0 < v_2^2(S) - v_1^2(S) < 2(\tau_2 - \tau_1)\bar{K},$$

which implies the continuity with respect to τ of v and consequently of w_τ. □

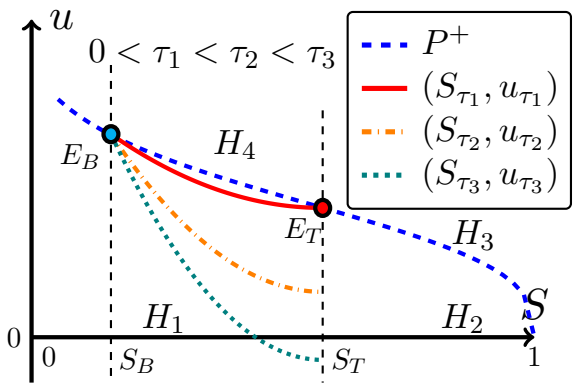

Figure 10: The dependence of the orbits (S_τ, u_τ) on τ for $S_B < S < S_T$.

From the discussion so far we conclude that the orbits (S_τ, u_τ) are close to the graph of P^+ for small values of τ, but move away from it as τ increases, and for $S \in (S_B, S_T]$. This situation is presented in Figure 10. In the remaining part of this subsection we focus on the behaviour of the system beyond the point $S = S_T$. The main goal is to show that orbits connecting E_B and E_T exist for all values of $\tau > 0$. In Theorem 4.1 we show this for small values of τ and for larger τ values the existence is shown in Theorems 4.2 and 4.3.

Theorem 4.1. *Let $\{(S_\tau, u_\tau)\}_{\tau>0}$ be the family of orbits of (4.7), (4.2), originating from E_B and entering H_1. Then there exists a $\tau_* > 0$ such that $w_{\tau_*}(S_T) = 0$. For all $\tau \in (0, \tau_*]$ the system (4.7), (4.2) has a unique orbit (S_τ, u_τ) satisfying $S_\tau(0) = (S_B + S_T)/2$ and connecting E_B and E_T.*

Proof. The existence of a τ_* for which $w_{\tau_*}(S_T) = 0$ follows directly from Propositions 4.2 and 4.3. Also, $w_\tau(S_T) < 0$ for $\tau > \tau_*$ and $w_\tau(S_T) > 0$ for $\tau < \tau_*$.

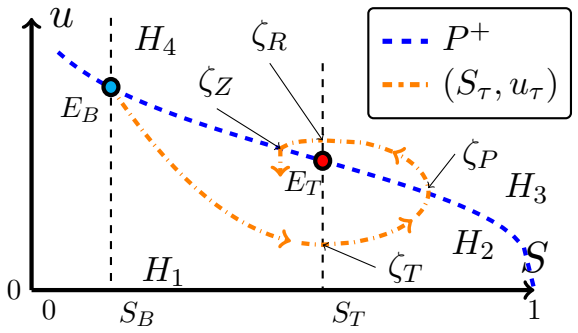

Figure 11: Behaviour of the orbit (S_τ, u_τ) for $\tau \le \tau_*$.

To understand the behaviour of (S_τ, u_τ) for $\tau < \tau_*$ we recall Proposition 4.1, which states that the orbit either approaches E_T or enters H_2 through $S = S_T$ at a finite ζ_T. In the latter case, which is displayed in Figure 11, u_τ becomes increasing for $\zeta > \zeta_T$. With $\tau < \tau_*$, since $P^+(1) = 0 < u_\tau(\zeta_T) < P^+(S_T)$ the orbit must intersect the graph of P^+ at some $\zeta = \zeta_P$ and enter H_3, where S_τ becomes decreasing whereas u_τ is still increasing. We claim that the orbit either approaches E_T, or enters H_4 for some $\zeta = \zeta_R$.

To see this, assume that a $\delta > 0$ exists such that $S_\tau(\zeta) \ge S_T + \delta$ for all $\zeta > \zeta_P$. As S_τ is bounded and decreasing, the limit $\lim_{\zeta\to\infty} S_\tau(\zeta)$ exists and is finite. Denoting it by $\tilde{S}_\tau$ we have $\tilde{S}_\tau \ge S_T + \delta$. Further, since u_τ is only bounded from below, a similar reasoning shows that either $\lim_{\zeta\to\infty} u_\tau(\zeta) = \tilde{u}_\tau \in [P^+(\tilde{S}_\tau), \infty)$ or $u_\tau \to \infty$.

Since S_τ is decreasing with ζ and bounded from below, $\lim_{\zeta\to\infty} S'_\tau = 0$. From (4.7) one gets $\tilde{u}_\tau = P^+(\tilde{S}_\tau)$. Therefore u_τ has a (finite) limit as $\zeta \to \infty$ and from (4.2) we get $\lim_{\zeta\to\infty} u'_\tau = 0$. In other words, $(\tilde{S}_\tau, \tilde{u}_\tau)$ is an equilibrium point, which is not possible since k is a convex function and therefore $\mathcal{G}$ has only two zeros. This rules out the possibility that S_τ is bounded away from S_T, so either $\lim_{\zeta\to\infty} S_\tau(\zeta) = S_T$, or the orbit enters H_4 at some finite argument ζ_R.

In the former case it follows as before that the orbit ends up in E_T. In the latter case we follow the arguments in Theorem 3.2 to prove that (S_τ, u_τ) cannot end up back in E_B, or leave H_4 through the line $S = S_B$. This means that it enters H_1 again at some $\zeta = \zeta_Z$. However, in this case the incoming part of the orbit is above the part emerging from E_B, and therefore the set bounded by $\{(S_\tau(\zeta), u_\tau(\zeta)) : \zeta < \zeta_Z\}$ and the graph of P^+ from E_B to $(S_\tau(\zeta_Z), u_\tau(\zeta_Z))$ is positive invariant. With this, the proof continues as in Theorem 3.2. □

Theorem 4.1 states that the orbits go to E_T for all $\tau \in (0, \tau_*]$ but it does not state how the orbits behave close to E_T. This is given in

Proposition 4.4. *There exists a $\tau_m > 0$ such that for $\tau \in (0, \tau_m]$ any orbit going to E_T goes either directly or after a finite number of turns around E_T, and for $\tau > \tau_m$ the orbit is a stable spiral around E_T.*

Proof. To prove this part we use the eigenvalues of the linearization around E_T, computed in (4.8). Let $\tau_m = \frac{k(S_T)(P^{+'}(S_T))^2}{4c(k'(S_T)-c)}$. Note that E_T is a stable sink for $0 < \tau \le \tau_m$ and a stable spiral for $\tau > \tau_m$. This proves the statement of Proposition 4.4. □

Having explained the behaviour of orbits close to E_T we again turn to existence, this time for $\tau > \tau_*$. As will be seen below, the orbits connecting E_B and E_T exist for $\tau > \tau_*$ too, but to

prove this we have to introduce

$$\alpha(S_B, S_T) = \int_{S_B}^{1} \mathcal{G}(\varrho; S_B, S_T) d\varrho. \tag{4.13}$$

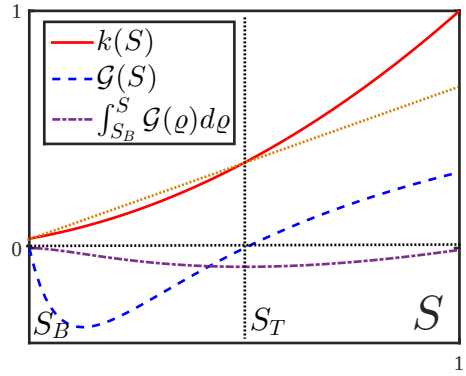

Figure 12: The functions k, $\mathcal{G}$, and the primitive of $\mathcal{G}$.

By the convexity of k, as stated in Assumption (A.1), and the definition $\mathcal{G}(S; S_B, S_B) = 1 - \frac{k'(S_B)(S-S_B)+k(S_B)}{k(S)}$, for any fixed $S \in (S_B, 1]$ the function $\mathcal{G}$ is decreasing with respect to $S_T \in (S_B, 1]$. Also, one has $\mathcal{G}(S; S_B, S_T) < 0$ if $S \in (S_B, S_T)$ and $\mathcal{G}(S; S_B, S_T) > 0$ if $S \in (S_T, 1]$. Moreover,

$$\alpha(S_B, 1) < 0 < \alpha(S_B, S_B), \tag{4.14}$$

and $\alpha(S_B, \cdot)$ is decreasing in $[S_B, S_T]$. Observe that $\alpha(S_B, S_T)$ does not depend on τ. Figure 12 shows how the functions $k(S)$, $\mathcal{G}(S)$ and $\int_{S_B}^{S} \mathcal{G}(\varrho; S_B, S_T) d\varrho$ vary with S .

With this we can now state the following

Theorem 4.2. *Let $S_B, S_T \in (0, 1]$, $S_B < S_T$ and $\alpha(S_B, S_T)$ be defined as above. If $\alpha(S_B, S_T) \geq 0$ then for all $\tau > \tau_*$ the orbit (S_τ, u_τ) reaches E_T as $\zeta \to \infty$.*

Proof. Since $\alpha(S_B, S_T) \geq 0$, by the properties of $\mathcal{G}$ an $S_\alpha \in [S_T, 1]$ exists such that

$$\int_{S_\alpha}^{1} \mathcal{G}(S; S_B, S_T) dS = \alpha(S_B, S_T). \tag{4.15}$$

Clearly, $S_\alpha < 1$ if $\alpha(S_B, S_T) > 0$ and $S_\alpha = 1$ if $\alpha(S_B, S_T) = 0$. Figure 13 (left) shows the location of S_α as the point where the hashed areas, below and above the S-axis, are equal. We rewrite (4.9) as

$$\frac{d}{dS}\left(P^+(S) w_\tau - \frac{1}{2} w_\tau^2\right) = c\tau \mathcal{G}(S) + w_\tau \frac{dP^+}{dS}. \tag{4.16}$$

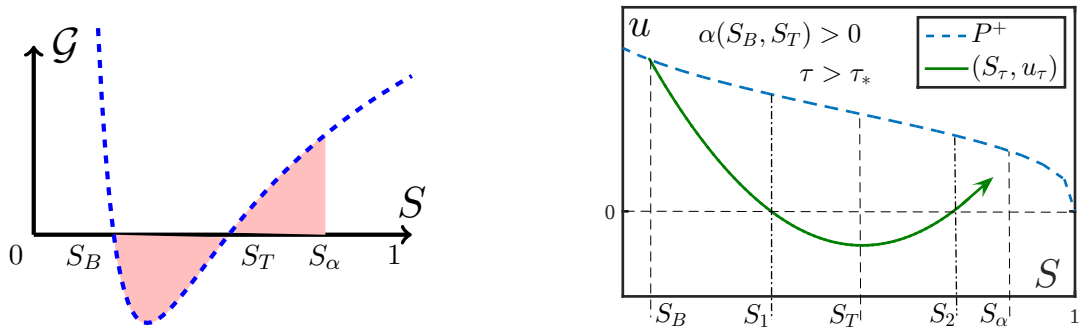

Figure 13: Left: S_α is the saturation at which the hashed area above the S-axis equals the one below the S-axis. Right: The (S_τ, u_τ) orbits for $\tau > \tau_*$ and $\alpha(S_B, S_T) > 0$. $S_1(\tau)$, $S_2(\tau)$ and S_α are shown in the image for this particular S_T value.

Since $\tau > \tau_*$, $w_\tau(S_T) < 0$. Let $S_1(\tau) \in (S_B, S_T)$ be such that $w_\tau(S) > 0$ for all $S \in [S_B, S_1(\tau))$, i.e. the first point where the orbit (S_τ, u_τ) enters the region $u < 0$. Observe that

w_τ is increasing for $S > S_T$. Further, let $S_2(\tau) \in (S_T, 1]$ be such that $w_\tau(S_2(\tau)) = 0$ and $w_\tau(S) < 0$ for all $S \in (S_1(\tau), S_2(\tau))$. We prove that $S_2(\tau) < 1$, thus the orbit returns in the upper half plane (see also Figure 13). More precisely, since $\alpha(S_B, S_T) \geq 0$, we prove in Proposition 4.6 that $S_2(\tau) < S_\alpha$ for all $\tau > \tau_*$.

Assume that $S_2(\tau) = 1$ for some $\tau > \tau_*$, then the domain of definition of w_τ can be extended to $[S_B, 1]$. Integrating (4.16) from $S_1(\tau)$ to 1 gives

$$-\frac{1}{2}w_\tau^2(1) = c\tau \int_{S_1}^1 \mathcal{G} + \int_{S_1}^1 w_\tau \frac{dP^+}{dS}.$$

Moreover, for $S \in (S_1(\tau), 1)$ one has $w_\tau(S) < 0$ and since $\mathcal{G}(S; S_B, S_T) < 0$ for $S \in (S_B, S_T)$ one has

$$\begin{aligned}\alpha &= \int_{S_B}^1 \mathcal{G}(S)dS = \int_{S_B}^{S_1} \mathcal{G} + \int_{S_1}^1 \mathcal{G} \\ &= \int_{S_B}^{S_1} \mathcal{G} - \frac{1}{2c\tau}w_\tau^2(1) - \frac{1}{c\tau}\int_{S_1}^1 w_\tau \frac{dP^+}{dS} < 0,\end{aligned}$$

which contradicts the assumption $\alpha(S_B, S_T) \geq 0$. Therefore, if $\tau > \tau_*$, a $S_2(\tau) \leq 1$ exists such that $w_\tau(S_2(\tau)) = 0$, meaning that the orbit (S_τ, u_τ) intersects the axis $u = 0$ for the second time. Following the reasoning in the proof of Theorem 4.1 one obtains that (S_τ, u_τ) ends up in E_T. □

The proof of Theorem 4.2 introduces three important values for the saturation, S_α given by (4.15), and $S_1(\tau)$, $S_2(\tau)$, the abscissas where the orbit intersects the axis $u = 0$. Below we give some results on the boundedness of w_τ, S_α and $S_2(\tau)$. We start with

Proposition 4.5. *Let $\tau > \tau_*$ be such that $S_2(\tau) \in (S_T, 1]$ exists. Then*

$$w_\tau(S_T) > -\underline{K}\sqrt{\tau},$$

where $\underline{K}^2 = 2c\int_{S_T}^1 \mathcal{G}(S)dS$

Proof. Equation (4.9) gives $(P^+(S) - w_\tau)w_\tau' = c\tau\mathcal{G}(S)$. As $w_\tau'(S) > 0$ for $S \in (S_T, S_2(\tau)]$, this gives $-w_\tau^{2\prime}(S) < 2c\tau\mathcal{G}(S)$. The proof follows by integrating this inequality over $(S_T, S_2(\tau)]$. □

Observe that the estimate in Proposition 4.5 gives a lower bound for w_τ since $w_\tau(S_T)$ is a minimum for w_τ. Also, the result does not require that $\alpha(S_B, S_T) \geq 0$.

The behaviour of S_α and $S_2(\tau)$ is stated in

Proposition 4.6. *Under the assumptions of Theorem 4.2, one has $S_2(\tau) < S_\alpha$ and $\lim_{\tau\to\infty} S_2(\tau) = S_\alpha$.*

Proof. To estimate $S_2(\tau)$ we integrate (4.16) from $S_1(\tau)$ to $S_2(\tau)$ and obtain

$$c\tau \int_{S_1(\tau)}^{S_2(\tau)} \mathcal{G}(S) + \int_{S_1(\tau)}^{S_2(\tau)} w_\tau \frac{dP^+}{dS} = 0.$$

Using this, one can split the integrals in (4.13) to obtain

$$\int_{S_2(\tau)}^1 \mathcal{G} = \alpha - \int_{S_B}^{S_1(\tau)} \mathcal{G} + \frac{1}{c\tau}\int_{S_1(\tau)}^{S_2(\tau)} w_\tau \frac{dP^+}{dS}. \tag{4.17}$$

Denoting by $I_1(\tau)$ and $I_2(\tau)$ the two integrals on the right, since $\mathcal{G} < 0$ for $S \in (S_B, S_T)$ and $w_\tau(S) < 0$ for $S \in (S_1(\tau), S_2(\tau))$ one gets $I_1(\tau) < 0$ and $I_2(\tau) > 0$. This gives $\int_{S_2(\tau)}^{S_\alpha} \mathcal{G} > 0$. As $S_2(\tau) > S_T$, $\mathcal{G} > 0$ for $S \in (S_2(\tau), 1)$ and therefore $S_2(\tau) < S_\alpha$ for all $\tau > \tau_*$.

To obtain the limit we start by proving that $S_1(\tau) \to S_B$ as $\tau \to \infty$. Clearly $S_1(\tau)$ decreases with increasing τ and remains bounded from below by S_B. Now suppose $S_1(\tau) \geq S_B + \delta$ for some $\delta > 0$ and for all $\tau > \tau_*$. Since $w_\tau(S) > 0$ and $\mathcal{G}(S) < 0$ for $S \in (S_B, S_1(\tau))$, integrating (4.9) from S_B to $S_1(\tau)$ gives

$$P^+(S_B) = c\tau \int_{S_B}^{S_1} \frac{-\mathcal{G}(S)}{P^+(S) - w_\tau(S)} dS > -\frac{c\tau}{P^+(S_B)} \int_{S_B}^{S_B+\delta} \mathcal{G}(S) dS.$$

This gives a contradiction for large τ as c and $\mathcal{G}$ do not depend on τ. Hence $\lim_{\tau\to\infty} I_1(\tau) = 0$.

To estimate I_2 we use Proposition 4.5 and the properties of w_τ

$$0 < I_2(\tau) = \frac{1}{c\tau} \int_{S_1}^{S_2} u_\tau \frac{dP^+}{dS} < \frac{1}{c\sqrt{\tau}} P^+(S_B) \underline{K}. \tag{4.18}$$

Hence $\lim_{\tau\to\infty} \int_{S_2}^1 \mathcal{G}(S) dS = \alpha = \int_{S_\alpha}^1 \mathcal{G}(S) dS$. This proves that $S_2 \to S_\alpha$ for $\tau \to \infty$. □

Having understood the behaviour of the orbits for the case $\alpha(S_B, S_T) \geq 0$ we proceed by analysing the case $\alpha(S_B, S_T) < 0$. In particular this situation occurs when S_T is close enough or equal to 1.

Lemma 4.1. *Let $S_B, S_T \in (0, 1]$, $S_B < S_T$ and $\alpha(S_B, S_T)$ introduced in (4.13). If $\alpha(S_B, S_T) < 0$ then a $\tau^* > \tau_*$ exists such that for all $\tau > \tau^*$, the orbit (S_τ, u_τ) passes through a point $(1, w_\tau(1))$ with $w_\tau(1) < 0$.*

Proof. We use ideas that are similar to the ones in the proof of Theorem 4.2. Assume that $S_2(\tau) \leq 1$ for all $\tau > \tau_*$. Integrating (4.16) from $S = S_B$ to $S = S_2(\tau)$ gives

$$\begin{aligned} -\frac{1}{2} P^+(S_B)^2 = c\tau \int_{S_B}^{S_2(\tau)} \mathcal{G}(S) + \int_{S_B}^{S_2(\tau)} w_\tau \frac{dP^+}{dS} &< c\tau\alpha + w_\tau(S_T)(P^+(S_2) - P^+(S_B)) \\ &< c\tau\alpha - w_\tau(S_T) P^+(S_B) < c\tau\alpha + P^+(S_B)\underline{K}\sqrt{\tau}. \end{aligned}$$

Since $\alpha < 0$ this gives a contradiction for τ exceeding a $\tau^* \geq \tau_*$, where τ^* is determined such that the term on the right in the equation above becomes equal to $-\frac{1}{2} P^+(S_B)^2$. From this it follows that for $\tau > \tau^*$ the orbit (S_τ, u_τ) has no second intersection point with the u-axis before passing through the vertical line $S = 1$, therefore $w_\tau(1) < 0$. □

From Lemma 4.1 we see that, if $\alpha(S_B, S_T) < 0$ and τ is large enough, the orbit (S_τ, u_τ) wants to exit the strip $[0, 1] \times \mathbb{R}$ through the half-line $\{(1, u) : u < 0\}$. However, the functions P^+ and k are only defined inside the physically relevant regime $S \in [0, 1]$ which makes the continuation of the orbits impossible and non-physical. Below we propose an extension of the model which allows continuation of the orbit within the physically relevant strip. It is based on the multi-valued extension of the P^+ curve,

$$P_e(S) = \begin{cases} P^+(S), & \text{for } 0 < S < 1, \\ (-\infty, 0] & \text{for } S = 1. \end{cases} \tag{4.19}$$

Such an approach is also used for defining extended pressure conditions in the case of porous media with block-type heterogeneities when models involving an entry pressure are adopted (see e.g. [9, 40]). With the extension the equations read

$$S' \in \frac{P_e(S) - u}{c\tau}, \tag{4.20}$$

$$u' = \mathcal{G}(S; S_B, S_T). \tag{4.21}$$

This formulation implies that if $S = 1$ in a set I of positive measure, then $S' = 0$ in I and $u \in P_e(1) = (-\infty, 0]$ in I. Moreover, from the u-equation,

$$u' = \mathcal{G}(1; S_B, S_T) \text{ in } I. \tag{4.22}$$

When $S_T = 1$ we have $\mathcal{G}(1; S_B, S_T) = 0$. Then any point on the half-line $\{S = 1\} \times \{-\infty < u \leq 0\}$ is an equilibrium point, and the compatibility condition $u = P^+(S_T)$ should be interpreted as $u_T \in P_e(1) = (-\infty, 0]$. We exploit this observation in the following construction.

$S_T < 1$

From Lemma 4.1 if $\tau > \tau^*$, the orbit (S_τ, u_τ) starting from E_B reaches $S = 1$ at finite $\zeta = \hat{\zeta}$ where $u_\tau(\hat{\zeta}) = \hat{u} < 0$. Then at $(1, \hat{u})$ we continue the orbit by the vertical upwards segment $\{1\} \times [\hat{u}, 0]$. Observe that along the segment, (4.20) and (4.21) are still satisfied. Since now $u' = \mathcal{G}(1; S_B, S_T) = \text{constant}$, we have $u' = \frac{\Delta u}{\Delta \zeta} = -\frac{\hat{u}}{\Delta \zeta} = \mathcal{G}(1; S_B, S_T) > 0$, yielding the length of the ζ interval when $S = 1$.

Now taking $(1, 0)$ as the starting point of (4.20) and (4.21) with $\zeta > \hat{\zeta} + \Delta\zeta$, we continue the construction as before. Again one uses the divergence argument from Theorem 3.2 to show that the orbit spirals into E_T. In particular the orbit cannot reach $S = 1$ for a second time as this would lead to a limit cycle which is ruled out from previous arguments.

$S_T = 1$

In this case the entire half-line $\{1\} \times (-\infty, 0]$ consists of equilibrium points. As before the orbit reaches $S = 1$ at finite $\zeta = \hat{\zeta}$, with $u = \hat{u} < 0$. But it stays at this point for all $\zeta \geq \hat{\zeta}$.

Summarising we have

Theorem 4.3. *Let τ^* be as in Lemma 4.1 and for any $\tau > \tau^*$ let (S_τ, u_τ) be the orbit satisfying* (4.20),(4.21) *emerging from E_B. Then*

(a) For $S_T < 1$ the orbit reaches $S = 1$ at finite $\zeta = \hat{\zeta}$ with $u(\hat{\zeta}) = \hat{u} < 0$. It continues along the segment $\{S = 1\} \times \{-\infty < u \leq 0\}$. At the point $(1, 0)$ it re-enters the set $\{S < 1\} \times \mathbb{R}$ and connects to E_T as $\zeta \to \infty$.

(b) For $S_T = 1$, again the orbit reaches $S = 1$ at finite $\zeta = \hat{\zeta}$ with $u(\hat{\zeta}) = \hat{u} < 0$. Since $(1, \hat{u})$ is an equilibrium, the orbit remains in this point for all $\zeta \geq \hat{\zeta}$.

Remark 4.1. To avoid non-physical saturation regimes, we have considered a multi-valued extension of the P^+-S curve. Whenever $S = 1$, the specific value of P_e is taken such that P_e and u are in equilibrium yielding $S' = 0$. For analysing the orbits in this case, one can also consider a regularised approximation of P_e. More precisely, with $\delta > 0$ being a small regularisation parameter, define

$$P_e^\delta(S) = \begin{cases} P^+(S) & \text{if } S < 1, \\ \frac{1}{\delta}(1 - S) & \text{if } S \geq 1 \end{cases}, \quad \mathcal{G}_e(S; S_B, S_T) = \begin{cases} \mathcal{G}(S; S_B, S_T) & \text{if } S < 1, \\ \mathcal{G}(1; S_B, S_T) & \text{if } S \geq 1. \end{cases} \tag{4.23}$$

Letting now $(S_\tau^\delta, u_\tau^\delta)$ be the orbits satisfying

$$\begin{cases} S' = \dfrac{P_e^\delta(S) - u}{c\tau}, \\ u' = \mathcal{G}_e(S; S_B, S_T), \end{cases} \tag{4.24}$$

and starting from E_B, one can analyze the behaviour of these orbits when $\delta \to 0$. In fact, this regularisation approach is being used for the numerical solutions presented in Section 5.

Having understood the above we can now distinguish the following situations which are shown in Figure 14. If $\alpha > 0$ the orbits stay away from $S = 1$ and approach E_T either directly or after spiraling (see Figure 14a). The situation is similar if $\alpha < 0$ and $\tau < \tau^*$. Whenever $\alpha < 0$ and $\tau > \tau^*$ then the orbit (S_τ, u_τ) has a vertical section at $S = 1$. The orbits (S_τ, u_τ) for $\alpha < 0$ are shown in Figure 14b.

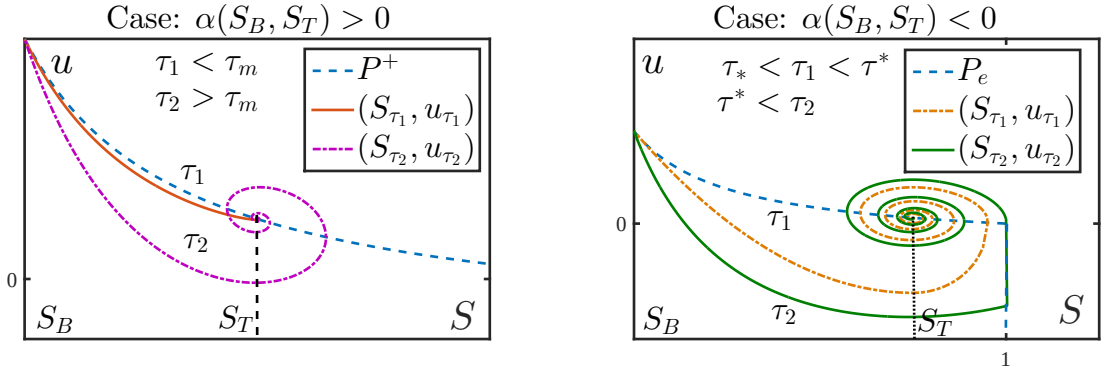

(a) Typical orbits for $\alpha(S_B, S_T) > 0$

(b) Typical orbits for $\alpha(S_B, S_T) < 0$

Figure 14: Behaviour of the orbits (S_τ, u_τ) for $\tau > 0$ and $f(S) = 1$.

We conclude this subsection by comparing the case $f \in L^1(0,1)$, $f \not\equiv 1$ to the case $f \equiv 1$. This means that one has to repeat the previous arguments for the system (4.4)-(4.5), now in terms of Y. With the functions introduced in (4.6), the direction of the orbits in the (Y, u) plane remains unaffected since $\tilde{\mathcal{G}}(Y; Y_B, Y_T) < 0$ for $Y_B < Y < Y_T$ and $\tilde{\mathcal{G}} \geq 0$ elsewhere in $(0, \infty)$ due to the convexity of k. The eigenvalues at (Y_B, u_B) and (Y_T, u_T) behave similarly: now the critical $\tau = \tilde{\tau}_m$ value at (Y_T, u_T) becomes

$$\tilde{\tau}_m = \frac{(\tilde{P}^{+\prime}(Y_T))^2}{4c\tilde{\mathcal{G}}'(Y_T)} = \frac{(P^{+\prime}(S_T))^2}{4c\mathcal{G}'(S_T)f(S_T)} = \frac{\tau_m}{f(S_T)}.$$

Propositions 4.1-4.3 remain valid, with the redefinition $\bar{K} = -c\int_{Y_B}^{Y_T} \tilde{\mathcal{G}}(Y)dY$. The existence Theorem 4.1 works also for this case, but now the divergence argument uses the function $\mathbf{F} = (\frac{1}{c\tau}(\tilde{P}^+(Y) - u), \tilde{\mathcal{G}}(Y))$, for which $\nabla \cdot \mathbf{F} = \frac{1}{c\tau}(\tilde{P}^+(Y))' = \frac{(P^+)'(S)}{c\tau f(S)} < 0$. Also, the parameter α given in (4.13), needs to be redefined as

$$\tilde{\alpha}(Y_B, Y_T) = \int_{Y_B}^{Y(1)} \tilde{\mathcal{G}}(Y; Y_B, Y_T)dY = \int_{S_B}^{1} f(S)\mathcal{G}(S; S_B, S_T)dS. \tag{4.25}$$

With this, the statement of Theorem 4.2 remains unchanged. Y_α, which corresponds to S_α defined in (4.15), can now be defined as

$$\int_{Y_\alpha}^{Y(1)} \tilde{\mathcal{G}}(Y; Y_B, Y_T)dY = \tilde{\alpha}(Y_B, Y_T). \tag{4.26}$$

Consequently, the new S_α satisfies $Y_\alpha = \int_0^{S_\alpha} f(S)dS$, or $\int_{S_B}^{S_\alpha} \mathcal{G}(S)f(S)dS = 0$. The constant $\underline{K}$ used in Propositions 4.5 and 4.6 becomes $\underline{K} = 2c\int_{Y_T}^{Y(1)} \tilde{\mathcal{G}}(Y)dY$. Lemma 4.1 remains the same. Finally, for proving Theorem 4.3 we now use the extension

$$\tilde{P}_e(Y) = \begin{cases} \tilde{P}^+(Y), & \text{for } 0 < Y < Y(1), \\ (-\infty, 0] & \text{for } Y = Y(1). \end{cases} \tag{4.27}$$

Following the arguments of Theorem 4.3 we get that Y reaches $Y(1)$ for a finite $\zeta = \tilde{\zeta}$ with $u(\tilde{\zeta}) = \tilde{u} < 0$ and depending upon whether $S_T < 1$ or $S_T = 1$ either the orbit reaches (Y_T, u_T) or stays at $(Y(1), \tilde{u})$.

4.2 The case when $f \notin L^1(0,1)$

The TW analysis of the dynamic capillarity model up to now is restricted to the case when $f \in L^1(0,1)$. This might not always be true. Since f is assumed continuous and positive on $[0,1)$, $f \notin L^1(0,1)$ implies that it becomes unbounded at $S = 1$. As will be proved below, in this case $S = 1$ is an upper bound for the saturation and the orbits remain inside the physically relevant regime $0 \le S \le 1$. This is like in the case $\alpha(S_B, S_T) < 0$ discussed before, but now extending the capillary pressure is not needed anymore.

Let $\delta > 0$ be arbitrarily small. Whenever $S \le 1 - \delta$, one can apply the transformation (4.3) to reduce the model (4.1)–(4.2) to the case analysed in Subsection 4.1 and most of the results there still remain valid. In particular, the orbits remain monotone if $S \in (S_B, S_T)$. The main difference appears close to $S = 1$, whenever this value is approached. We have

Theorem 4.4. *Assume $f \notin L^1(0,1)$ and let $\tau > 0$, $S_B \in (0,1)$, $S_T \in (S_B, 1]$ be given. For the orbits (S_τ, u_τ) leaving E_B one has*

(a) If $S_T < 1$, then $S_\tau(\zeta) < 1$ for all $\zeta \in \mathbb{R}$.

(b) If $S_T = 1$, then two cases can occur.

(b.1) If $f\mathcal{G} \notin L^1(0,1)$ then as $\zeta \to \infty$, $S_\tau \to 1$ and $u_\tau \to -\infty$.

(b.2) If $f\mathcal{G} \in L^1(0,1)$ then there exists a $u^* \in (-\infty, P^+(1)]$ such that $\lim_{\zeta\to\infty}(S_\tau, u_\tau) \to (1, u^*)$.

Proof. (a) Assume first that $S_T < 1$. Compared to the situation analysed in Theorem 4.1, the differences appear whenever S_τ approaches 1. We therefore focus on part of the orbit satisfying $S_\tau > S_T$. In this case, $u_\tau' > 0$ whereas $S_\tau' > 0$ as long as the orbit (S_τ, u_τ) stays below the P^+ curve. Two situations are possible: the orbit either intersects the P^+ curve for some argument ζ_3, or it reaches the line $S = 1$.

In the former situation, let $S_{3,\tau} = S_\tau(\zeta_3)$. We know that $S_\tau(\zeta) \le S_{3,\tau}$ for all $\zeta \in \mathbb{R}$, so if $S_{3,\tau} < 1$ then the proof is completed. Assuming the contrary, namely that a $\tau_0 > 0$ exists such that $S_{3,\tau_0} = 1$, one has $u_{\tau_0}(\zeta_3) \le P^+(1)$ and (4.9) gives

$$\frac{dw_\tau}{dS}(S) = \frac{\tau c f(S)\mathcal{G}(S)}{P^+(S) - w_\tau}. \tag{4.28}$$

As $P^{+\prime}(S) < 0$ and $\mathcal{G}(S) > 0$ for $S \in [S_T, 1)$ one uses (4.11) to see that $P^+ - w_{\tau_0} \ge 0$ decreases

for $S \in [S_T, 1]$. Further, integration of (4.10) gives (with redefinition $\bar{K} = -c\int_{S_B}^{S_T} f(\varrho)\mathcal{G}(\varrho)d\varrho$

$$\begin{aligned}\sqrt{2\tau_0\bar{K}} &> P^+(S_T) - w_{\tau_0}(S_T) > w_{\tau_0}(1) - w_{\tau_0}(S_T)\\ &= \int_{S_T}^1 \frac{\tau_0 c f(S)\mathcal{G}(S)}{P^+(S) - w_{\tau_0}(S)}dS \geq \frac{\tau_0 c}{P^+(S_T) - w_{\tau_0}(S_T)}\int_{S_T}^1 f(S)\mathcal{G}(S)dS\\ &\geq \frac{\tau_0 c}{P^+(S_T) - w_{\tau_0}(S_T)}\int_{\frac{S_T+1}{2}}^1 f(S)\mathcal{G}(S)dS \geq \frac{c\tau_0 m_{\mathcal{G}}}{P^+(S_T) - w_{\tau_0}(S_T)}\int_{\frac{S_T+1}{2}}^1 f(S)dS,\end{aligned}$$

with $m_{\mathcal{G}} = \min\{\mathcal{G}(S), \frac{1}{2}(S_T+1) \leq S \leq 1\}$. Since $m_{\mathcal{G}} > 0$ and $f \notin L^1(S_B, 1)$, the integral on the right is unbounded, which gives a contradiction.

The second case, when the orbit reaches the line $S = 1$, can be ruled out by similar arguments. We omit the details here.

(*b*) For $S_T = 1$, observe that $S_\tau'(\zeta) > 0$ for $(S_\tau, u_\tau) \in H_1$ and S_τ is bounded above by 1 following the arguments used for proving Corollary 3.1. Consequently S_τ has a limit S_∞ for $\zeta \to \infty$. Assume $S_\infty < 1$. We know that $u_\tau'(\zeta)$ decreases monotonically for $\zeta \in \mathbb{R}$ so that there are two possibilities. If $\lim_{\zeta\to\infty} u_\tau(\zeta) = u_\infty > -\infty$ then from (4.1) and (4.2) it follows that S_τ' and u_τ' both have a limit as $\zeta \to \infty$. Moreover, since S_τ and u_τ have horizontal asymptotes, it means that $\lim_{\zeta\to\infty} S_\tau'(\zeta) = \lim_{\zeta\to\infty} u_\tau'(\zeta) = 0$. From (4.2) we then get $\mathcal{G}(S_\infty) = 0$, contradicting $S_\infty < 1$. On the contrary, if $\lim_{\zeta\to\infty} u_\tau(\zeta) = -\infty$ then from (4.2) we get

$$S_\tau'(\zeta) = \frac{P^+(S) - u_\tau(\zeta)}{c\tau f(S)} \geq \frac{P^+(S)}{c\tau f(S)} \geq \inf_{S\in[S_B, S_\infty]}\left\{\frac{P^+(S)}{c\tau f(S)}\right\} > 0,$$

for all $\zeta > M_\zeta$ with some large enough M_ζ. This means that S_τ cannot have a limit $S_\infty < 1$. Therefore the only possibility remaining is $\lim\limits_{\zeta\to\infty} S_\tau = S_\infty = 1$.

Now let us consider the case $f\mathcal{G} \notin L^1(0,1)$. Observe that since $\mathcal{G} < 0$ for $S \in (S_B, 1)$ one has $\int_{S_B}^1 f(-\mathcal{G}) = \infty$. If w_τ tends to $u^* > -\infty$ then integrating (4.28) from S_B to 1 and multiplying by -1 we get

$$P^+(S_B) - u^* = \int_{S_B}^1 \frac{-\tau c f(S)\mathcal{G}(S)}{P^+(S) - w_\tau(S)}dS > \frac{\tau c}{P^+(S_B) - u^*}\int_{S_B}^1 f(S)(-\mathcal{G}(S))dS,$$

which is a contradiction since the term on the left is bounded whereas the integral on the right is not. Hence $\lim_{S\to 1} w_\tau = -\infty$.

Next, for $f\mathcal{G} \in L^1(0,1)$ after redefining $\bar{K}$ as $\bar{K} = -c\int_{S_B}^1 \mathcal{G}f$, Proposition 4.2 gives a lower bound for $w_\tau(S_T)$ that is uniform for all $S_B < S_T \leq 1$. Also observe that for a fixed S_B, $w_\tau(S; S_B, S_T)$ are well ordered with respect to S_T meaning that for $S_B < S_{T,1} < S_{T,2} < 1$, $w_\tau(S; S_B, S_{T,1}) > w_\tau(S; S_B, S_{T,2})$ in their common domain of definition. To see why this holds observe that for $S \in (S_B, S_{T,1})$ and $u < P^+(S)$,

$$\frac{\tau c f(S)\mathcal{G}(S; S_B, S_{T,1})}{P^+(S) - u} > \frac{\tau c f(S)\mathcal{G}(S; S_B, S_{T,2})}{P^+(S) - u}$$

with $\mathcal{G}(S; S_B, S_{T,1}) > \mathcal{G}(S; S_B, S_{T,2})$ following from the convexity of k. Using (4.28) and proceeding as in the proof of Theorem 3.1 we conclude that the orbits are well-ordered in $S \in (S_B, S_{T,1})$ with respect to S_T. As $w_\tau(S; S_B, S_{T,1}) > w_\tau(S_{T,1}; S_B, S_{T,1})$ for $S > S_{T,1}$, the well ordering holds throughout the common domain of definition. In view of the boundedness of $w_\tau(S_T)$ mentioned before, $\lim_{S_T\to 1} w_\tau(S_T; S_B, S_T) = u^* > -\infty$. Finally proceeding like proof of Corollary 3.1 one proves that this value can be only attained as $\zeta \to \infty$. □

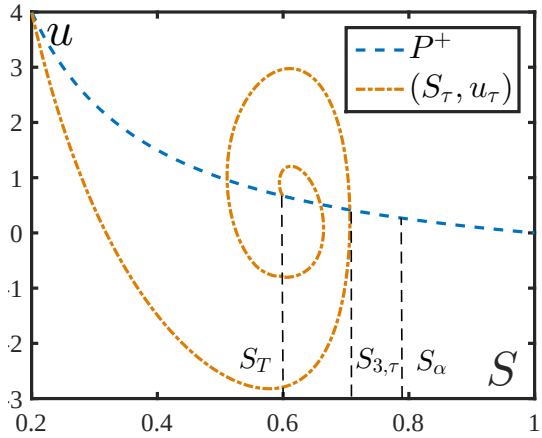

Figure 15: Typical (S_τ, u_τ) orbit for the case $f \notin L^1(0,1)$, $S_T < 1$.

From the proof above we see that in the case $S_T < 1$, for any $\tau > 0$ the orbit may turn around the equilibrium E_T without reaching the line $S = 1$. In particular, an $S_{3,\tau} \in (S_T, 1)$ exists such that the orbit interescts the graph of P^+ for the first time after E_B in the point $(S_{3,\tau}, P^+(S_{3,\tau}))$, see Figure 15. Moreover, since $f \in C(0,1)\backslash L^1(0,1)$ whereas $\mathcal{G} \in C[0,1]$ with $\mathcal{G}(1) > 0$ one has $\lim_{S \nearrow 1} \int_{S_B}^{S} f(z)\mathcal{G}(z)dz = \infty$. Since $\mathcal{G} < 0$ on (S_B, S_T), a unique $S_\alpha \in (S_T, 1)$ exists such that

$$\int_{S_B}^{S_\alpha} f(S)\mathcal{G}(S)dS = 0.$$

Observe that this simply extends the definition of S_α in (4.13), given for the case $f \equiv 1$ to $f \in L^1(0,1)$ and $f \notin L^1(0,1)$. Having introduced the above, as in the case $f \equiv 1$, it is interesting to see what happens if τ becomes very large. We have:

Corollary 4.1. *Let $S_T < 1$ and S_α, $S_{3,\tau}$ be as introduced above. Then $\lim_{\tau\to\infty} S_{3,\tau} = S_\alpha$.*

Proof. As in the proof of Proposition 4.3, the orbits are ordered with respect to τ. Therefore $S_{3,\tau}$ is increasing with respect to τ and bounded from above, $S_{3,\tau} < 1$. Hence there exists the limit $\lim_{\tau\to\infty} S_{3,\tau} = S_3^*$. As in Theorem 4.2, for $\tau > \tau_*$ and $S > S_T$ let $S_{2,\tau}$ be the abscissa where the orbit intersects the axis $u = 0$. Following the argument in Theorem 4.2, one proves that $\lim_{\tau\to\infty} S_{2,\tau} = S_\alpha$. Also as $S_{3,\tau} > S_{2,\tau}$ it is easy to see that $S_3^* \geq S_\alpha$. Now integrating (4.28) from $S_{2,\tau}$ to $S_{3,\tau}$ gives □

$$P^+(S_T) > w_\tau(S_{3,\tau}) = \int_{S_{2,\tau}}^{S_{3,\tau}} \frac{\tau c f(S)\mathcal{G}(S)}{P^+(S) - w_\tau(S)} dS \geq \frac{\tau c}{P^+(S_T)} \int_{S_{2,\tau}}^{S_{3,\tau}} f(S)\mathcal{G}(S)dS.$$

Observe that if $S_3^* > S_\alpha$, since $\lim_{\tau\to\infty} S_{3,\tau} = S_3^*$ the integral on the right becomes positive for τ large enough. On the other hand, since the term on the left is bounded, as $\tau \to \infty$ this integral must approach 0. For $S_3^* > S_\alpha$ this gives a contradiction, so the only possibility is that $S_3^* = S_\alpha$.

Remark 4.2. For $S_T < 1$, Corollary 4.1 shows that for all $\tau > 0$ the orbits remain at the left of $S = S_\alpha < 1$. This means that the travelling waves exist without needing to extend the capillary pressure in the non-physical domain $S > 1$.

Remark 4.3. Observe that τ and f have different effects. Specifically, changing τ affects the orbit for all values of ζ, whereas f plays a major role only in the vicinity of $S = 1$.

5 Numerical results

The numerical results presented in this section complement the theoretical findings in the previous sections. Specifically, after solving numerically the system (2.9), (2.12) we verify the predictions made in previous sections for sufficiently large times. In the numerical calculations we take a simple relative permeability function, $k(S) = S^2$. The other nonlinear functions are specified later.

5.1 Numerical Scheme

We start by presenting the numerical scheme. Below $\varepsilon > 0$ and $\tau \geq 0$ are fixed. With $S_B < S_T$ we consider the system given by (2.9),(2.12) for $t > 0$ and $x \in (-\ell, \ell)$. The space interval is taken large enough to allow the saturation and pressure to develop profiles resembling the travelling wave profiles. In all cases, $\ell \geq 50$.

For the numerical solution we first discretize in time (2.9) and (2.12). Let $\Delta t > 0$ be the time step and let $t_n = n\Delta t$ for $n \in \mathbb{N}$. The time discrete unknowns S_n, u_n approximate the saturation and pressure at t_n. We introduce the function $\mathcal{F}$ which gives the discretization of $\partial_t S$. One gets from (2.12) that $\mathcal{F}(S,u) = c\Phi_\varepsilon\left(\frac{P^+(S)-u}{P^-(S)}\right)$ for the hysteresis case and $\mathcal{F}(S,u) = \frac{1}{c\tau}(P_e^\delta(S) - u)$ for the dynamic capillarity case. With the $\mathcal{F}$-notation, the explicit discretisation of (2.12) reads

$$S_n = S_{n-1} + \Delta t \mathcal{F}(S_{n-1}, u_{n-1}). \tag{5.1}$$

For stability we solve the time discrete version of (2.9) implicitly,

$$\partial_x\left(k(S_n)\partial_x u_n\right) = -\mathcal{F}(S_n, u_n) - \partial_x k(S_n), \tag{5.2}$$

together with the pressure boundary conditions at $x = \pm\ell$,

$$u_n(-\ell) = u_T, \quad u_n(\ell) = u_B. \tag{5.3}$$

For the spatial discretisation we use standard finite differences.

Observe that for $n = 0$, u_0 is obtained from (5.2) by using the initial condition for saturation, S_0. The saturation initial condition is C^1 approximation of the Riemann data and it is consistent with the boundary conditions. Specifically $S_0 : [-\ell, \ell] \to (0,1)$ satisfies

$$S_0(x) = S_T, \text{ if } x \leq -\ell_1, \quad \text{ respectively } S_0(x) = S_B \text{ if } x \geq \ell_1. \tag{5.4}$$

Here $\ell_1 << \ell$ is a positive number, and S_T and S_B are compatible with the corresponding pressure values, i.e. $p_i = P^+(S_i)$ $(i \in \{B,T\})$. Here $\ell_1 = 5$. Inside $(-\ell_1, \ell_1)$ we take $S_0(x) = \frac{(S_B+S_T)}{2} + \frac{(S_T-S_B)}{4\ell_1^3}x(x^2 - 3\ell_1^2)$. It is to be noted that the choice S_0 does not have considerable impact on the end results as long as the necessary assumptions are satisfied.

As a validation of the numerical results, we compare the propagation speed of the numerical profile with the Rankine-Hugoniot speed given in (2.21). The profile speed is calculated as the speed of the point $x_f(t)$ at which $S(x_f(t), t) = \frac{1}{2}(S_B + S_T)$. By (2.22), $\zeta = 0$ at this point, meaning that $x_f(t) = ct$. Figure 16a presents the results for the hysteresis case, which agrees with the TW speed up to the discretisation error. The results for the dynamic capillarity model are similar. We emphasise the fact that all results presented below are numerical approximations of the solutions of the original system of partial differential equations and do not assume any TW structure. Nevertheless, for t long enough the numerical solutions obtained for the specified initial and boundary conditions develop profiles resembling closely the TW solutions.

5.2 Iterative scheme

Observe that the equation (5.2) is nonlinear in u_n for the capillary hysteresis case and so an linear iterative scheme has to be used to solve for u_n. For the Φ_ε function defined in Proposition 3.1, the iterative schemes show poor convergence properties particularly because $|\partial_u \mathcal{F}(S,u)|$ can become unbounded in this case in two different ways. Firstly, if $u \to p_{imb}(S)$ or $u \to p_{drn}(S)$, then $|\partial_u \mathcal{F}(S,u)| \to \infty$. To resolve this we define Φ_ε on $\mathbb{R}$ in a way such that $\Phi'_\varepsilon(r) = \frac{1}{\varepsilon}$ for $|r| > 1$. Note that this Φ_ε is different from the function Φ_ε given in Proposition 3.1, but satisfies Assumption (A.4). This particular choice guarantees the numerical convergence of the nonlinear problem (5.2).

Secondly, $|\partial_u \mathcal{F}(S,u)| \to \infty$ if $S \to 0$ or $S \to 1$. This problem is avoided by taking $S_B > 0$ and $S_T < 1$. So when studying the case $S_T = 1$, we actually show the result for the limit $S_T \nearrow 1$. With these modifications, $\mathcal{F}$ becomes locally Lipschitz in both variables S and u for a fixed $\varepsilon > 0$.

Because Φ'_ε becomes unbounded as $\varepsilon \to 0$, iterative schemes like Newton's method fail to converge because of the requirement of having good initial guesses. Therefore to solve (5.2) we use a linear iteration scheme inspired by the L-scheme discussed in [36, 38]. Specifically, for a sufficiently large L that will be specified later and with i as the iteration index, we solve the linear elliptic equation

$$L u_n^i - \partial_x \left(k(S_n) \partial_x u_n^i \right) = L u_n^{i-1} + \mathcal{F}(S_n, u_n^{i-1}) + \partial_x k(S_n). \tag{5.5}$$

Following the arguments from [36, 38] one can show that if $L \geq L_{\min} > 0$, the scheme in (5.5) becomes a contraction and converges irrespective of the initial guess. However, a natural choice is to start with $u_n^0 = u_{n-1}$. The lower bound $L_{\min}$ is the Lipschitz constant of $\mathcal{F}$ with respect to the variable u.

(a) (b)

Figure 16: Convergence study for the hysteresis model. The parameters are $S_B = 0.2$, $S_T = 0.6$, $\Delta x = .1$, $\Delta t = 10^{-3}$, $\varepsilon = 10^{-3}$ unless specified otherwise.
(a) x_f as a function of t, where x_f is the x-location at which $S(x_f,t) = \frac{1}{2}(S_B + S_T)$. According to (2.21) the TW speed should be $c = \frac{dx_f}{dt} = 0.8$. From the figure we get $\frac{dx_f}{dt} = 0.7892$.
(b) Error $(\log_{10}(\|u_n^i - u_n^{i-1}\|_{L^2([-\ell,\ell])}))$ vs iterations for different ε and Δx pairs.

Note that the choice of L is left open, under the restriction $L \geq L_{\min}$. For the hysteresis case, $L_{\min}$ behaves like $\frac{1}{\varepsilon}$, which leads to very slow convergence of the scheme [36]. At the same time, in large parts of the time-space cylinder $(0,\infty) \times (-\ell,\ell)$, the values of S and u are such that $\Phi'_\varepsilon = \mathcal{O}(\varepsilon)$, and therefore using a constant $L = O(\varepsilon^{-1})$ is inefficient. To improve the local convergence of the scheme, in the numerical calculations we have taken a variable L, namely $L(x,t_n) := 2\partial_u \mathcal{F}(S_{n-1}(x), u_{n-1}(x))$ in every control volume.

The iterative process is stopped if the L^2 norm of the difference between two iterates decreases below 10^{-10}. Following [36, 38], the convergence is linear regardless of the mesh size.

This can be seen in Figure 16, where the convergence of the iterative process is shown for the hysteresis model.

Capillary Hysteresis

We start by presenting the results for the capillary hysteresis case. The primary drainage and imbibition curves are taken such that

$$P^+(S) = \left(\frac{1-S}{S}\right), \quad \text{and} \quad P^-(S) = 2(1-S)^2. \tag{5.6}$$

With $b = \sqrt[3]{\varepsilon}$ and $a = (1 - (\varepsilon^2)^{\frac{2}{3}})$, the function Φ_ε used in the numerical scheme is

$$\Phi_\varepsilon(r) = \begin{cases} b + \frac{1}{\varepsilon}(r-1) & \text{for } r > 1 \\ \varepsilon r(1-ar^2)^{-1/2} & \text{for } r \in [-1,1] \\ -b + \frac{1}{\varepsilon}(r+1) & \text{for } r < -1 \end{cases}.$$

The case $S_T = 1$ was studied first. Observe that in this case the model degenerates whenever S approaches 1, where P^- vanishes. To avoid this degeneracy, the calculations were performed for an S_T slightly less than 1. This yields monotone profiles of S and u, as shown in Figure 17, and is in good agreement with the TW profiles for $S_T = 1$. The right plot presents the pair $(S_\varepsilon(x,t), u_\varepsilon(x,t))$ in the S-u plane, for a fixed t and $x \in (-\ell, \ell)$. In analogy with the dynamical system analysis for the TW solutions, we call this an "orbit". We use this term to refer to all similar plots that will be presented below.

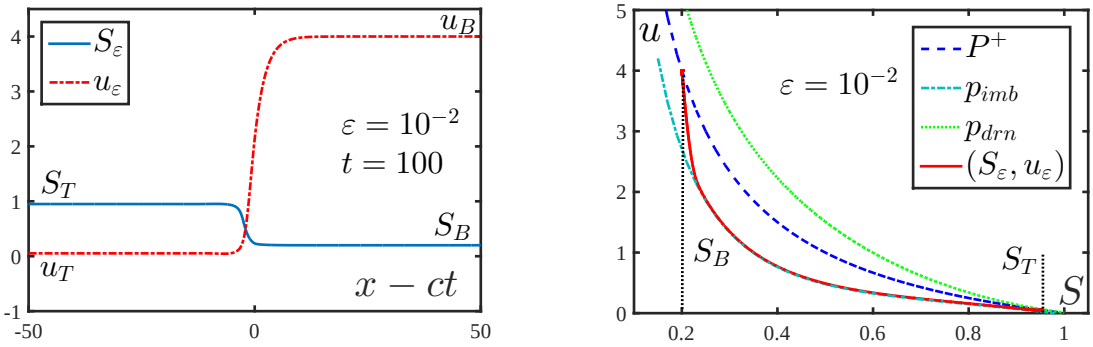

Figure 17: Left: the profiles of S_ε and u_ε in the transformed coordinate $x - ct$ (left); right: the orbit $(S_\varepsilon, u_\varepsilon)$ for the hysteresis model in the limit case $S_T \uparrow 1$. The figures are obtained for $S_T = .97$, $S_B = 0.2$, $\Delta x = .1$, $\Delta t = 10^{-3}$.

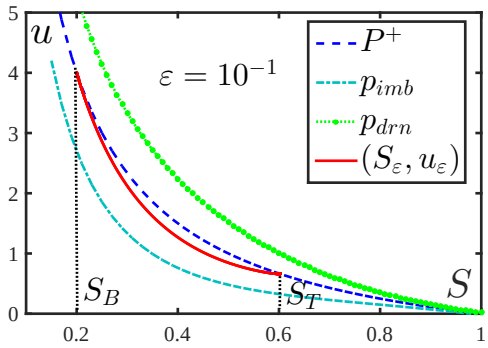

Figure 18: The orbit $(S_\varepsilon, u_\varepsilon)$ for $S_B = 0.2$, $S_T = 0.6$, $\Delta x = .1$, $\Delta t = 10^{-3}$ and $\varepsilon = 10^{-1}$.

Next we consider the $S_T < 1$ case. We fix $S_T = 0.6$ and $S_B = 0.2$ and vary ε. Figure 18 shows the results for $\varepsilon = 10^{-1}$. Observe that the orbit is monotone and E_T is a stable sink. According to Theorem 3.2b, E_T becomes a spiral sink as ε becomes small enough. This is indeed the situation displayed in Figure 19, obtained for $\varepsilon = 10^{-2}$. We clearly see that the (numerical) orbit spirals toward E_T. Consequently, for t sufficiently large, the profiles of u_ε and S_ε are non-monotone.

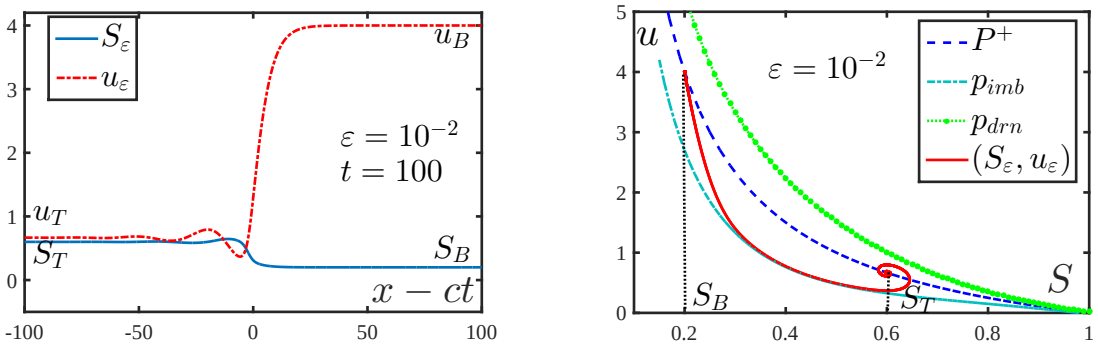

Figure 19: Left: the profiles of S_ε and u_ε in the transformed coordinate $x - ct$; right: the orbit $(S_\varepsilon, u_\varepsilon)$ for $\varepsilon = 10^{-2}$. The other parameters are $S_B = 0.2$, $S_T = 0.6$, $\Delta x = .1$, $\Delta t = 10^{-3}$.

The results for $\varepsilon = 10^{-3}$ are similar, as shown in Figure 20. However, when compared to the case $\varepsilon = 10^{-2}$ a longer time is required until the numerical solutions develop a profile resembling the travelling waves. To explain this, we observe that whenever $p_{imb}(S) < u < p_{drn}(S)$ one has $\partial_t S = H_\varepsilon\left(\frac{P^+(S)-u}{P^-(S)}\right) \approx \varepsilon H_1\left(\frac{P^+(S)-u}{P^-(S)}\right)$. Therefore the time required for a profile to develop to a travelling wave profile scales with $\frac{1}{\varepsilon}$. Also note that close to $S = S_B$, the numerical orbit for $\varepsilon = 10^{-3}$ has a steeper profile than the one for $\varepsilon = 10^{-2}$. This is in agreement with Corollary 3.1.

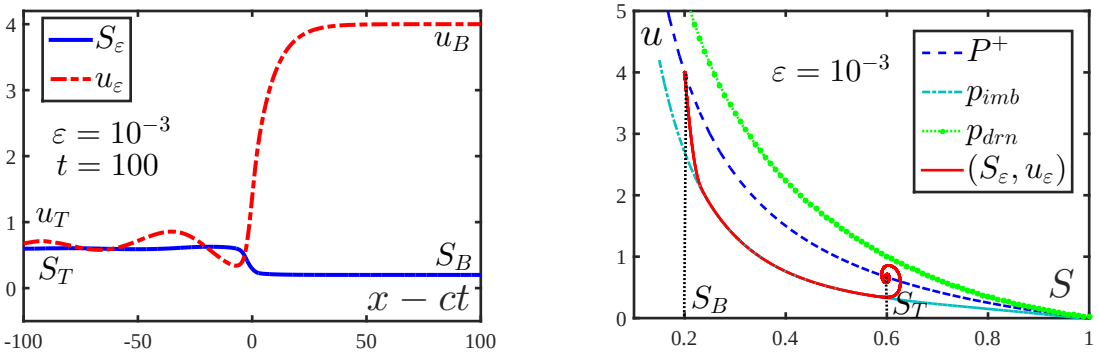

Figure 20: Results for $\varepsilon = 10^{-3}$. The other parameters are as in Figure 19.

Another observation is that the oscillations in the S and u profiles are wider for $\varepsilon = 10^{-3}$ than for $\varepsilon = 10^{-2}$. This also follows from Remark 3.1, stating that the period of oscillation scales with $\mathcal{O}(\varepsilon^{-1/2})$. Lastly one can see that the amplitude of oscillations in saturation for $\varepsilon = 10^{-3}$ is less than that of $\varepsilon = 10^{-2}$. This follows from Proposition 3.5. This can be seen in the S–u phase plane as well: the S-range of the spirals decreases with ε. Therefore we conclude that the numerical results are in good agreement with the TW analysis for the hysteresis mmodel.

Dynamic Capillarity

The numerical results for the dynamic capillarity model are obtained for the quadratic function k and the P^+ function given in (5.6). Recall that in this case the two primary curves, drainage and imbibition, are equal. This mans that P^- is vanishing.

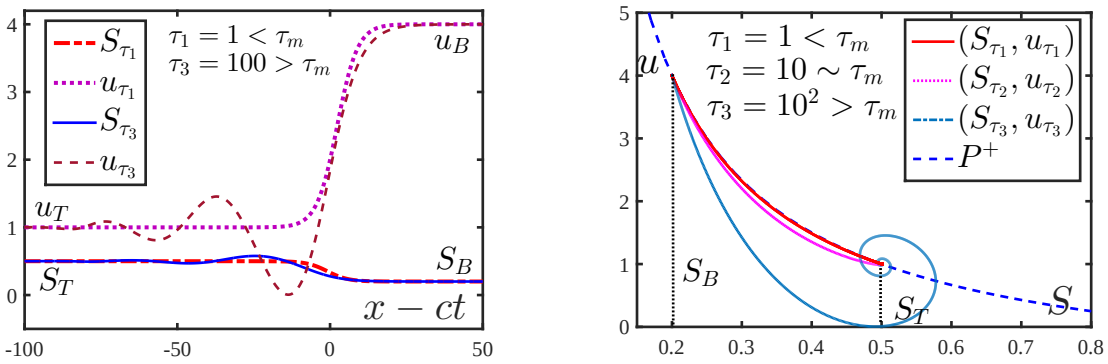

Figure 21: Left: the profiles of S_τ and u_τ in the transformed coordinate $x - ct$; right: the orbit (S_τ, u_τ) for different τ values. The τ values used are $\tau_1 = 1$, $\tau_2 = 10$ and $\tau_3 = 100$. The other parameters are $S_B = 0.2$, $S_T = 0.5$, $\Delta x = .1$, $\Delta t = 10^{-3}$. In this case $\alpha(S_B, S_T) > 0$.

We first take $f(S) = 1$. Figure 21 displays results in the case $S_B = 0.2$ and $S_T = 0.5$, when $\alpha(S_B, S_T) > 0$. By Proposition 4.4, a τ_m exists such that for $\tau < \tau_m$ the profiles of S and u are monotone, and for $\tau > \tau_m$ they are non-monotone as E_T becomes a spiral sink. The value τ_3 in Figure 21 is taken so that $w_{\tau_3}(S_T) \approx 0$. Also, a case with $\tau \sim \tau_m$ is shown. In this case no oscillations are observed and the orbit goes directly to E_T. These behaviours agree with the results given in Propositions 4.2,4.3 and 4.4.

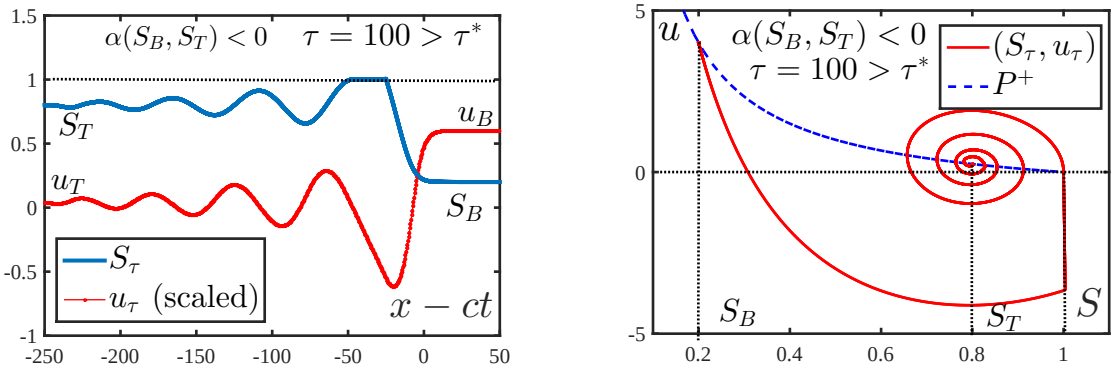

Figure 22: Left: the profiles of S_τ and u_τ in the transformed coordinate $x - ct$ with $\tau = 100 > \tau^*$ and $\alpha(S_B, S_T) < 0$; right: the orbit (S_τ, u_τ) in the (S, u) plane. Here $S_B = 0.2$, $S_T = 0.8$. The regularised extended model (4.24) given in Remark 4.1 has been used for this computation with a δ value of 10^{-3} used in P_e^δ (see (4.23)).

Next we take the case $S_B = 0.2$ and $S_T = 0.8$, in which case $\alpha(S_B, S_T) < 0$. To avoid the unphysical saturation regimes we have considered extended P_e-S model given in (4.20),(4.21). However, for the numerical solution this multi-valued extension is replaced by the regularised P_e^δ-S curve given in (4.23) with $\delta = 10^{-3}$. Figure 22 shows the profiles and orbits for $\tau > \tau^*$. Observe that, due to the regularisation, S is still exceeding 1 and for $S \geq 1$ the orbit is not vertical but has a steep slope. As $\delta \to 0$ the possibility of having $S > 1$ is eliminated and the orbit goes vertically along $S = 1$. Moreover, in this case pressure remains continuously differentiable, but a kink can be observed at the transition from $S = 1$ to $S < 1$ which is as one expects from extension (4.24) given in Remark 4.1. Therefore we claim that the results are in good agreement with the theory.

Finally, we investigate the case when $f \notin L^1(0,1)$. We choose $f(S) = \frac{1}{1-S}$ with $S_B = 0.2$, $S_T = 0.8$. The results are given in Figure 23. The profile takes considerably more time to develop and hence a kink is still visible in Figure 23 as a remnant of the initial condition. Compared to the case $f \in L^1(0,1)$, we observe that the saturation stays below $S = 1$, but as τ increases the saturation approaches S_α, which for Figure 23 is $S_\alpha = 0.9903$. This is in good agreement with the results in Theorem 4.4 and Corollary 4.1.

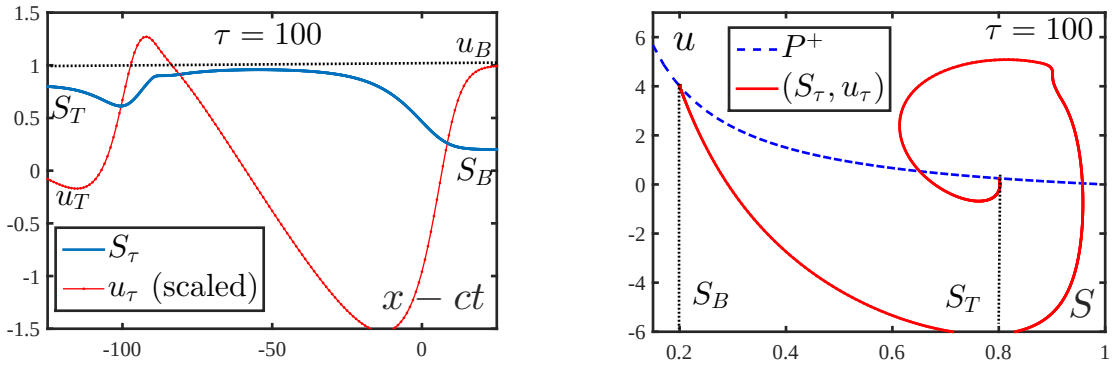

Figure 23: Left: the profiles of S_τ and u_τ in the transformed coordinate $x - ct$ for the case $f \notin L^1(0,1)$; right: the orbit (S_τ, u_τ). Here $f(S) = \frac{1}{1-S}$ with $S_B = 0.2$, $S_T = 0.8$ and $\tau = 100$. The value of S_α in this case is calculated to be $S_\alpha = 0.9903$.

6 Conclusion

In this paper we discussed the implications of including non-equilibrium effects in unsaturated porous flow models. Specifically, the play-type hysteresis and dynamic capillarity effects are considered in the saturation-pressure relationship. One focus was on analysing the occurrence of non-monotonic saturation or pressure profiles (overshoots) arising due to the non-equilibrium effects mentioned above. To this end, the traveling wave analysis is considered to understand the flow in a long, homogeneous vertical porous column.

The analysis is done first for hysteresis models. In this case, the existence of travelling wave solutions was shown first for the regularized case and then for the limiting case, leading to a play-type hysteresis model. It was proved that oscillations may appear in the regularised hysteresis models, which correspond to non-vertical scanning curves. However, in the limit situation these oscillations disappear and the saturation-pressure orbits lie on the imbibition curve.

Next we have investigated the dynamic capillarity effects, for which the existence of TW solutions is proved. Furthermore, the existence of a threshold value for the dynamic capillarity parameter is shown so that for values less than this the travelling waves are monotonic, and become non-monotonic for values above the threshold. Moreover, similar thresholds are found for the dynamic capillary parameter that dictates whether the overshoot will have regions of positive pressure or whether the overshoot will reach a maximum corresponding to the full saturation. Also mechanisms to restrict the saturation to physically relevant values are analysed.

Finally, a semi-implicit numerical scheme to solve the nonlinear, pseudo parabolic equations corresponding to the non-equilibrium model was proposed. For solving the emerging time discrete, nonlinear equations, an L-scheme was used. This scheme is used for solving the original partial differential equation in a large, but finite domain. For sufficiently large times the numerical solutions show a good resemblance with the travelling wave profiles predicted theoretically.

Acknowledgment

C.J. van Duijn acknowledges the support of the Darcy Centre of Utrecht University and Eindhoven University of Technology. K. Mitra is supported by Shell and the Netherlands Organisation for Scientific Research (NWO) through the CSER programme (project 14CSER016) and by the Hasselt University through the project BOF17BL04. The research of I.S. Pop is supportde by the Research Foundation-Flanders (FWO) through the Odysseus programme (project G0G1316N). The authors thank the anonymous referees for their careful reading of the manuscript and their valuable comments.

References

[1] Abreu, E., and Vieira, J., Computing numerical solutions of the pseudo-parabolic Buckley-Leverett equation with dynamic capillary pressure, Mathematics and Computers in Simulation 137 (2017): 29-48

[2] Bedjaoui, N., and LeFloch, P.G., Diffusive-dispersive traveling waves and kinetic relations. I. Nonconvex hyperbolic conservation laws. Journal of Differential Equations 178 (2002): 574-607

[3] Beliaev, A.Y, and Hassanizadeh, S.M., A theoretical model of hysteresis and dynamic effects in the capillary relation for two-phase flow in porous media, Transport in Porous Media 43 (2001): 487-510

[4] Beliaev, A.Y., and Schotting, R.J. , Analysis of a new model for unsaturated flow in porous media including hysteresis and dynamic effects, Computational Geosciences 5.4 (2001): 345-368

[5] Bertsch, M., Smarrazzo, F., and Tesei, A., Pseudoparabolic regularization of forward-backward parabolic equations: a logarithmic nonlinearity. Analysis & PDE 6.7 (2013): 1719-1754.

[6] Böhm, M., and Showalter, R.E., A nonlinear pseudoparabolic diffusion equation. SIAM Journal on Mathematical Analysis 16.5 (1985): 980-999

[7] Bottero, S., Hassanizadeh, S.M., Kleingeld, P.J., and Heimovaara, T.J., Nonequilibrium capillarity effects in two-phase flow through porous media at different scales, Water Resources Research 47.10 (2011)

[8] Bourgeat, A., and Panfilov, M., Effective two-phase flow through highly heterogeneous porous media: Capillary nonequilibrium effects, Computational Geosciences 2.3 (1998): 191-215

[9] Brenner, K., Cancès, C., and Hilhorst, D., Finite volume approximation for an immiscible two-phase flow in porous media with discontinuous capillary pressure, Computational Geosciences 17.3 (2013): 573-597

[10] Brokate, M., Botkin, N.D., and Pykhteev, O.A., Numerical simulation for a two-phase porous medium flow problem with rate independent hysteresis, Physica B: Condensed Matter 407.9 (2012): 1336-1339

[11] Cancès, C., Choquet, C. , Fan, Y., and Pop, I.S., An existence result related to two-phase flows with dynamical capillary pressure, CASA Report 10-75, Eindhoven University of Technology (2010)

[12] Cao, X., and Pop, I.S., Degenerate two-phase porous media flow model with dynamic capillarity, Journal of Differential Equations 260.3 (2016): 2418-2456

[13] Cao, X., and Pop, I.S., Two-phase porous media flows with dynamic capillary effects and hysteresis : uniqueness of weak solutions, Computers & Mathematics with Applications 69.7 (2015): 688-695

[14] Cao, X., and Pop, I.S., Uniqueness of weak solutions for a pseudo-parabolic equation modeling two phase flow in porous media, Applied Mathematics Letters 46 (2015): 25-30

[15] Collins, R.E., Flow of fluids through porous materials, Petroleum Publishing Company (1976)

[16] Corli, A., Rohde, C., and Schleper, V., Parabolic approximations of diffusive-dispersive equations, Journal of Mathematical Analysis and Applications 414.2 (2014): 773-798

[17] Cuesta, C., van Duijn, C.J., and Hulshof, J., Infiltration in porous media with dynamic capillary pressure: travelling waves, European Journal of Applied Mathematics 11.4 (2000): 381-397

[18] DiCarlo, D.A., Experimental measurements of saturation overshoot on infiltration, Water Resources Research 40.4 (2004): W04215

[19] DiCarlo, D.A., Juanes, R., LaForce, T., and Witelski, T.P., Nonmonotonic traveling wave solutions of infiltration into porous media, Water Resources Research 44.2 (2008): W02406

[20] Doster, F., Zegeling, P., and Hilfer, R., Numerical solutions of a generalized theory for macroscopic capillarity, Physical Review E 81.3 (2010): 036307

[21] Egorov, A.G., Dautov, R.Z., Nieber, J.L., and Sheshukov, A.Y., Stability analysis of gravity-driven infiltrating flow, Water Resources Research 39.9 (2003): 1266

[22] Hassanizadeh, S.M., and Gray, W.G., Thermodynamic basis of capillary pressure in porous media, Water Resources Research 29.10 (1993): 3389-3405

[23] Helmig, R., Weiss, A., and Wohlmuth, B.I., Dynamic capillary effects in heterogeneous porous media, Computational Geosciences 11.3 (2007): 261-274

[24] Hilfer, R., and Steinle, R., Saturation overshoot and hysteresis for two phase flow in porous media, The European Physical Journal Special Topics 223 (2014): 2323-2338

[25] Koch, J., Rätz, A., and Schweizer, B., Two-phase flow equations with a dynamic capillary pressure, European Journal of Applied Mathematics 24.1 (2013): 49-75

[26] Manthey, S., Hassanizadeh, S.M., Helmig, R., and Hilfer, R., Dimensional analysis of two-phase flow including a rate-dependent capillary pressure-saturation relationship, Advances in Water Resources 31.9 (2008): 1137-1150

[27] Milišić, J.P., The unsaturated flow in porous media with dynamic capillary pressure, arXiv preprint arXiv: 1703.10662 (2017)

[28] Mikelić, A., A global existence result for the equations describing unsaturated flow in porous media with dynamic capillary pressure, Journal of Differential Equations 248.6 (2010): 1561-1577

[29] Morrow, N.R., and Harris, C.C., Capillary equilibrium in porous materials, Society of Petroleum Engineers Journal 5.01 (1965): 15-24

[30] Niessner, J., and Hassanizadeh, S.M. , A model for two-phase flow in porous media including fluid-fluid interfacial area, Water Resources Research 44.8 (2008)

[31] Nordbotten, J.M., and Celia, M.A., Geological storage of CO2: modeling approaches for large-scale simulation, Wiley (2011)

[32] Papafotiou, A., Sheta, H., and Helmig, R., Numerical modeling of two-phase hysteresis combined with an interface condition for heterogeneous porous media, Computational Geosciences 14.2 (2010): 273-287

[33] Parker, J.C., and Lenhard, R.J., A Model for hysteretic constitutive relations governing multiphase flow: 1. Saturation pressure relations. Water Resources Research 23.12 (1987): 2187-2196

[34] Plohr, B., Marchesin, D., Bedrikovetsky, P., and Krause, P., Modeling hysteresis in porous media flow via relaxation, Computational Geosciences 5.3 (2001): 225-256

[35] Pop, I.S., van Duijn, C.J., Niessner, J., and Hassanizadeh, S.M., Horizontal redistribution of fluids in a porous medium: The role of interfacial area in modeling hysteresis, Advances in Water Resources 32.3 (2009): 383-390

[36] Pop, I.S., Radu, F., and Knabner, P., Mixed finite elements for the Richards' equation: linearization procedure, Journal of Computational and Applied Mathematics 168.1 (2004): 365-373

[37] Quarteroni, A., Sacco, R., and Saleri, F., Numerical Mathematics, Springer-Verlag (2000)

[38] Radu, F., Kumar, K., Nordbotten, J.M., and Pop, I.S., A robust, mass conservative scheme for two-phase flow in porous media including Hölder continuous nonlinearities, IMA Journal of Numerical Analysis (2017): drx032

[39] Rätz, A., and Schweizer, B., Hysteresis models and gravity fingering in porous media, Zeitschrift für Angewandte Mathematik und Mechanik 94 (2014): 645-654

[40] Schweizer, B., Homogenization of degenerate two-phase flow equations with oil-trapping, SIAM Journal on Mathematical Analysis 39.6 (2008): 1740-1763

[41] Schweizer, B., The Richards equation with hysteresis and degenerate capillary pressure, Journal of Differential Equations 252.10 (2012), 5594-5612

[42] Schweizer, B., Instability of gravity wetting fronts for Richards equations with hysteresis, Interfaces and Free Boundaries 14.1 (2012): 37-64

[43] Schweizer, B., Laws for the capillary pressure in a deterministic model for fronts in porous media, SIAM Journal on Mathematical Analysis 36.5 (2005): 1489-1521

[44] Shearer, M., Spayd, K.R., and Swanson E.R., Traveling waves for conservation laws with cubic nonlinearity and BBM type dispersion, Journal of Differential Equations 259.7 (2015): 3216-3232

[45] Szymkiewicz, A., Modelling water flow in unsaturated porous media, Springer (2013)

[46] Van Duijn, C.J., Fan, Y., Peletier, L.A., and Pop, I.S., Travelling wave solutions for degenerate pseudo-parabolic equations modelling two-phase flow in porous media, Nonlinear Analysis: Real World Applications 14.3 (2013): 1361-1383

[47] Van Duijn, C.J., and Knabner, P., Travelling waves during the transport of reactive solute in porous media: combination of Langmuir and Freundlich isotherms, Advances in Water Resources 16.2 (1993): 97-105

[48] Van Duijn, C.J., and Mitra, K., Hysteresis and horizontal redistribution in porous media, CMAT Report UP-17-05, Hasselt University (2017)

[49] Van Duijn, C.J., Peletier, L.A., and Pop, I.S., A new class of entropy solution of the Buckley-Leverett equation, SIAM Journal on Mathematical Analysis 39.2 (2007): 507-536

[50] Van Genuchten, M.T., A closed form equation for predicting the hydraulic conductivity of unsaturated soils, Soil Science Society of America Journal 44.5 (1980): 894-897

[51] Visintin, A., Differential model of hysteresis, Springer (1994)

[52] Zhang, H., and Zegeling, P.A., A numerical study of two-phase flow models with dynamic capillary pressure and hysteresis, Transport in Porous Media 116.2 (2017): 825-846

[53] Zhuang, L., Advanced theories of water redistribution and infiltration in porous media: Experimental studies and modeling, Doctoral dissertation, Utrecht University, Department of Earth Sciences (2017)